### Lactate Production Assay

Cells were plated in 24-well plate and cultured overnight. After pretreated with or without 10 μM LY294002, cells were treated with EGF (50 ng/ml) for 8 hr. Culture medium was removed from cells and lactate concentration was determined using lactate test strips and Accutrend Lactate analyzer (Accutrend Lactate, Roche). Next, cells were harvested, stained with trypan blue, and viable cell numbers were counted directly under the microscope using hemocytometer. Last, the rate of lactate production were determined (lactate production rate = lactate concentration/cells/time) and normalized with the rate detected in control group.

### In Vivo Tumorigenesis Assay and In Vivo Glucose Uptake Assay

For in vivo tumorigenesis assays, $5 \times 10^6$ of BT-474-M1 cells were injected into mammary fat pad of age-matched athymic female nude mice (five mice for each group). Tumor size was measured weekly with a caliper, and tumor volume was determined with the standard formula: $L \times W^2 \times 0.52$, where L is the longest diameter and W the shortest diameter. While developed tumors reached to the volume ~200 $mm^3$, mice were imaged and analyzed with [$^{18}$F] FDG for in vivo glucose uptake. [$^{18}$F]FDG were administered via a single tail-vein injection and PET/CT images were scanned and collected on Inveon CT/PET system (Siemens). Mice were awake during the uptake period and maintained on a heating pad. Images were then reconstructed using two-dimensional ordered subsets expectation maximization (OSEM) algorithm. PET and CT image fusion and image analysis were performed using software ASIPro 5.2.4.0 (Siemens). For Herceptin treatment, $8 \times 10^6$ of BT-474-M1 cells were injected into mammary fat pad of age-matched athymic female nude mice (five mice for each group). While developed tumors have reach to the volume around 200 $mm^3$, mice were injected with 5 mg/kg of Herceptin or vehicle control (IgG) intraperitoneally once per week, and tumor size was measured weekly with a caliper.

### Cell Growth Assay

For Herceptin administration, $8 \times 10^3$ of BT-474 cells with control, Skp2 knockdown were seeded in 12-wells in triplicate, 24 hr later, treated with Herceptin (refreshed every 2 days). Six days later, cells were harvested, stained with trypan blue, and viable cells were counted directly under the microscope using hemocytometer.

### Immunohistochemistry and Scoring

The procedures of immunohistochemical studies were performed as previously described (Huang et al., 2006). In brief, sections were cut onto an adhesive-coated glass slides at 3-μm thickness. For stainings in human samples, the slides were incubated with primary antibodies targeting Her-2 (Thermo Scientific, Clone SP3, 1:100), Skp2 (Invitrogen, clone 2C8D9, 1:100), and pAkt$^{(Ser473)}$ (Cell Signaling, clone D9E, 1:25). The slides from mouse samples were incubated with primary antibodies for pAkt$^{(Ser473)}$ (Cell Signaling, clone D9E, 1:25), Ki-67 (Abcam, polyclonal, 1:200), and Glut1 (Abcam, clone SPM498, 1:200), respectively. Primary antibodies were detected using the ChemMate DAKO EnVision kit (DAKO, K5001). The slides were incubated with the secondary antibody for 30 min and developed with 3,3-diaminobenzidine for 5 min. Incubation without the primary antibody was used as a negative control. Immunoexpression was scored by two pathologists (C.F.L and H.Y.H.) using a multiheaded microscope to reach a consensus for each case. The staining was evaluated based on a combination of both the percentage and intensity of positively stained tumor cells to generate an H-score, which was calculated using the following equation: H-score = $\Sigma Pi\,(i + 1)$, where $i$ is the intensity of the stained tumor cells (0 to 4 +), and $Pi$ is the percentage of stained tumor cells for each intensity.

### Statistical Analysis

Statistical analyses were performed using the SPSS 14 software package. For human breast samples, the Mann-Whitney U test was used to assess the differential expression level of Skp2 and pAkt$^{(S473)}$ expression in relation to Her-2 expression status. The Spearman's rank correlation coefficient was used to clarify the association between Skp2 expression to clinicopathological variables and pAkt$^{(Ser473)}$ expression levels. The endpoint analyzed was distal metastasis-free survival, calculated from the starting date of surgery to the date of event. The median period of follow-up was 103 months (range, 6–143). Survival analysis was performed using the Cox proportional hazards model. Survival curves were plotted using the Kaplan-Meier method, and log-rank tests were performed to evaluate prognostic differences between groups for categorical variables. For mouse samples, the expression levels of pAkt, Ki-67, and Glut1 between various groups were assessed by using Mann-Whitney U test. For all analyses, two-sided tests of significance were used with $p = <0.05$ considered significant.

## SUPPLEMENTAL INFORMATION

Supplemental Information includes Extended Experimental Procedures, seven figures, and four tables and can be found with this article online at doi:10.1016/j.cell.2012.02.065.

## ACKNOWLEDGMENTS

We thank Mrs. J. Delacerda and C.V. Kingsley at small animal imaging facility of MD Anderson Cancer Center for their assistance in CT/PET imaging. We also thank the members from Lin's laboratory for their valuable comments and suggestions. We thank Drs. W. Tansey and M. H. Lee for reagents. This work was supported by the MD Anderson Cancer Center Trust Scholar Award, Prostate SPORE Career Development Award (P50 CA140388 SPORE), NIH grants, CPRIT grant, DOD prostate cancer New Investigator Award (H.K.L.), the MD Anderson Cancer Center Breast SPORE Career Development Award (C.H.C.), the Susan G. Komen Breast Cancer Foundation postdoctoral fellowship (C.H.C.), and a grant from the Department of Health in Taiwan (C.F.L.).

Received: August 31, 2011
Revised: January 6, 2012
Accepted: February 28, 2012
Published: May 24, 2012

## REFERENCES

Agus, D.B., Akita, R.W., Fox, W.D., Lewis, G.D., Higgins, B., Pisacane, P.I., Lofgren, J.A., Tindell, C., Evans, D.P., Maiese, K., et al. (2002). Targeting ligand-activated ErbB2 signaling inhibits breast and prostate tumor growth. Cancer Cell *2*, 127–137.

Aragonés, J., Fraisl, P., Baes, M., and Carmeliet, P. (2009). Oxygen sensors at the crossroad of metabolism. Cell Metab. *9*, 11–22.

Barthel, A., Okino, S.T., Liao, J., Nakatani, K., Li, J., Whitlock, J.P., Jr., and Roth, R.A. (1999). Regulation of GLUT1 gene transcription by the serine/threonine kinase Akt1. J. Biol. Chem. *274*, 20281–20286.

Birnbaum, M.J. (2004). On the InterAktion between hexokinase and the mitochondrion. Dev. Cell *7*, 781–782.

Bornstein, G., Bloom, J., Sitry-Shevah, D., Nakayama, K., Pagano, M., and Hershko, A. (2003). Role of the SCFSkp2 ubiquitin ligase in the degradation of p21Cip1 in S phase. J. Biol. Chem. *278*, 25752–25757.

Brazil, D.P., Park, J., and Hemmings, B.A. (2002). PKB binding proteins. Getting in on the Akt. Cell *111*, 293–303.

Chan, C.H., Lee, S.W., Li, C.F., Wang, J., Yang, W.L., Wu, C.Y., Wu, J., Nakayama, K.I., Kang, H.Y., Huang, H.Y., et al. (2010a). Deciphering the transcriptional complex critical for RhoA gene expression and cancer metastasis. Nat. Cell Biol. *12*, 457–467.

Chan, C.H., Lee, S.W., Wang, J., and Lin, H.K. (2010b). Regulation of Skp2 expression and activity and its role in cancer progression. ScientificWorldJournal *10*, 1001–1015.

Chan, C.H., Gao, Y., Moten, A., and Lin, H.K. (2011). Novel ARF/p53-independent senescence pathways in cancer repression. J. Mol. Med. (Berl.) *89*, 857–867.

Datta, K., Franke, T.F., Chan, T.O., Makris, A., Yang, S.I., Kaplan, D.R., Morrison, D.K., Golemis, E.A., and Tsichlis, P.N. (1995). AH/PH domain-mediated interaction between Akt molecules and its potential role in Akt regulation. Mol. Cell. Biol. *15*, 2304–2310.

DeBerardinis, R.J., Lum, J.J., Hatzivassiliou, G., and Thompson, C.B. (2008). The biology of cancer: metabolic reprogramming fuels cell growth and proliferation. Cell Metab. *7*, 11–20.

Elstrom, R.L., Bauer, D.E., Buzzai, M., Karnauskas, R., Harris, M.H., Plas, D.R., Zhuang, H., Cinalli, R.M., Alavi, A., Rudin, C.M., and Thompson, C.B. (2004). Akt stimulates aerobic glycolysis in cancer cells. Cancer Res. *64*, 3892–3899.

Gao, D., Inuzuka, H., Tseng, A., Chin, R.Y., Toker, A., and Wei, W. (2009). Phosphorylation by Akt1 promotes cytoplasmic localization of Skp2 and impairs APCCdh1-mediated Skp2 destruction. Nat. Cell Biol. *11*, 397–408.

Huang, H.Y., Kang, H.Y., Li, C.F., Eng, H.L., Chou, S.C., Lin, C.N., and Hsiung, C.Y. (2006). Skp2 overexpression is highly representative of intrinsic biological aggressiveness and independently associated with poor prognosis in primary localized myxofibrosarcomas. Clin. Cancer Res. *12*, 487–498.

Hynes, N.E., and MacDonald, G. (2009). ErbB receptors and signaling pathways in cancer. Curr. Opin. Cell Biol. *21*, 177–184.

Jiang, B.H., Jiang, G., Zheng, J.Z., Lu, Z., Hunter, T., and Vogt, P.K. (2001). Phosphatidylinositol 3-kinase signaling controls levels of hypoxia-inducible factor 1. Cell Growth Differ. *12*, 363–369.

Kim, S.Y., Herbst, A., Tworkowski, K.A., Salghetti, S.E., and Tansey, W.P. (2003). Skp2 regulates Myc protein stability and activity. Mol. Cell *11*, 1177–1188.

Künstle, G., Laine, J., Pierron, G., Kagami Si, S., Nakajima, H., Hoh, F., Roumestand, C., Stern, M.H., and Noguchi, M. (2002). Identification of Akt association and oligomerization domains of the Akt kinase coactivator TCL1. Mol. Cell. Biol. *22*, 1513–1525.

Lee-Hoeflich, S.T., Crocker, L., Yao, E., Pham, T., Munroe, X., Hoeflich, K.P., Sliwkowski, M.X., and Stern, H.M. (2008). A central role for HER3 in HER2-amplified breast cancer: implications for targeted therapy. Cancer Res. *68*, 5878–5887.

Lin, H.K., Bergmann, S., and Pandolfi, P.P. (2004). Cytoplasmic PML function in TGF-beta signalling. Nature *431*, 205–211.

Lin, H.K., Wang, G., Chen, Z., Teruya-Feldstein, J., Liu, Y., Chan, C.H., Yang, W.L., Erdjument-Bromage, H., Nakayama, K.I., Nimer, S., et al. (2009). Phosphorylation-dependent regulation of cytosolic localization and oncogenic function of Skp2 by Akt/PKB. Nat. Cell Biol. *11*, 420–432.

Lin, H.K., Chen, Z., Wang, G., Nardella, C., Lee, S.W., Chan, C.H., Yang, W.L., Wang, J., Egia, A., Nakayama, K.I., et al. (2010). Skp2 targeting suppresses tumorigenesis by Arf-p53-independent cellular senescence. Nature *464*, 374–379.

Liu, P., Cheng, H., Roberts, T.M., and Zhao, J.J. (2009). Targeting the phosphoinositide 3-kinase pathway in cancer. Nat. Rev. Drug Discov. *8*, 627–644.

Majumder, P.K., Febbo, P.G., Bikoff, R., Berger, R., Xue, Q., McMahon, L.M., Manola, J., Brugarolas, J., McDonnell, T.J., Golub, T.R., et al. (2004). mTOR inhibition reverses Akt-dependent prostate intraepithelial neoplasia through regulation of apoptotic and HIF-1-dependent pathways. Nat. Med. *10*, 594–601.

Manning, B.D., and Cantley, L.C. (2007). AKT/PKB signaling: navigating downstream. Cell *129*, 1261–1274.

Nakayama, K.I., and Nakayama, K. (2006). Ubiquitin ligases: cell-cycle control and cancer. Nat. Rev. Cancer *6*, 369–381.

Nakayama, K., Nagahama, H., Minamishima, Y.A., Matsumoto, M., Nakamichi, I., Kitagawa, K., Shirane, M., Tsunematsu, R., Tsukiyama, T., Ishida, N., et al. (2000). Targeted disruption of Skp2 results in accumulation of cyclin E and p27(Kip1), polyploidy and centrosome overduplication. EMBO J. *19*, 2069–2081.

Noguchi, M., Ropars, V., Roumestand, C., and Suizu, F. (2007). Proto-oncogene TCL1: more than just a coactivator for Akt. FASEB J. *21*, 2273–2284.

Oshima, R.G., Lesperance, J., Munoz, V., Hebbard, L., Ranscht, B., Sharan, N., Muller, W.J., Hauser, C.A., and Cardiff, R.D. (2004). Angiogenic acceleration of Neu induced mammary tumor progression and metastasis. Cancer Res. *64*, 169–179.

Osthus, R.C., Shim, H., Kim, S., Li, Q., Reddy, R., Mukherjee, M., Xu, Y., Wonsey, D., Lee, L.A., and Dang, C.V. (2000). Deregulation of glucose transporter 1 and glycolytic gene expression by c-Myc. J. Biol. Chem. *275*, 21797–21800.

Pelicano, H., Martin, D.S., Xu, R.H., and Huang, P. (2006). Glycolysis inhibition for anticancer treatment. Oncogene *25*, 4633–4646.

Plas, D.R., and Thompson, C.B. (2005). Akt-dependent transformation: there is more to growth than just surviving. Oncogene *24*, 7435–7442.

Robey, R.B., and Hay, N. (2009). Is Akt the "Warburg kinase"?-Akt-energy metabolism interactions and oncogenesis. Semin. Cancer Biol. *19*, 25–31.

Shim, H., Dolde, C., Lewis, B.C., Wu, C.S., Dang, G., Jungmann, R.A., Dalla-Favera, R., and Dang, C.V. (1997). c-Myc transactivation of LDH-A: implications for tumor metabolism and growth. Proc. Natl. Acad. Sci. USA *94*, 6658–6663.

van de Vijver, M.J., He, Y.D., van't Veer, L.J., Dai, H., Hart, A.A., Voskuil, D.W., Schreiber, G.J., Peterse, J.L., Roberts, C., Marton, M.J., et al. (2002). A gene-expression signature as a predictor of survival in breast cancer. N. Engl. J. Med. *347*, 1999–2009.

Vander Heiden, M.G., Cantley, L.C., and Thompson, C.B. (2009). Understanding the Warburg effect: the metabolic requirements of cell proliferation. Science *324*, 1029–1033.

von der Lehr, N., Johansson, S., Wu, S., Bahram, F., Castell, A., Cetinkaya, C., Hydbring, P., Weidung, I., Nakayama, K., Nakayama, K.I., et al. (2003). The F-box protein Skp2 participates in c-Myc proteosomal degradation and acts as a cofactor for c-Myc-regulated transcription. Mol. Cell *11*, 1189–1200.

Wang, H., Bauzon, F., Ji, P., Xu, X., Sun, D., Locker, J., Sellers, R.S., Nakayama, K., Nakayama, K.I., Cobrinik, D., and Zhu, L. (2010). Skp2 is required for survival of aberrantly proliferating Rb1-deficient cells and for tumorigenesis in Rb1+/- mice. Nat. Genet. *42*, 83–88.

Warburg, O. (1956). On the origin of cancer cells. Science *123*, 309–314.

Wieman, H.L., Wofford, J.A., and Rathmell, J.C. (2007). Cytokine stimulation promotes glucose uptake via phosphatidylinositol-3 kinase/Akt regulation of Glut1 activity and trafficking. Mol. Biol. Cell *18*, 1437–1446.

Xia, Z.P., Sun, L., Chen, X., Pineda, G., Jiang, X., Adhikari, A., Zeng, W., and Chen, Z.J. (2009). Direct activation of protein kinases by unanchored polyubiquitin chains. Nature *461*, 114–119.

Yang, W.L., Wang, J., Chan, C.H., Lee, S.W., Campos, A.D., Lamothe, B., Hur, L., Grabiner, B.C., Lin, X., Darnay, B.G., and Lin, H.K. (2009). The E3 ligase TRAF6 regulates Akt ubiquitination and activation. Science *325*, 1134–1138.

Yang, W.L., Wu, C.Y., Wu, J., and Lin, H.K. (2010a). Regulation of Akt signaling activation by ubiquitination. Cell Cycle *9*, 487–497.

Yang, W.L., Zhang, X., and Lin, H.K. (2010b). Emerging role of Lys-63 ubiquitination in protein kinase and phosphatase activation and cancer development. Oncogene *29*, 4493–4503.

Zeng, W., Sun, L., Jiang, X., Chen, X., Hou, F., Adhikari, A., Xu, M., and Chen, Z.J. (2010). Reconstitution of the RIG-I pathway reveals a signaling role of unanchored polyubiquitin chains in innate immunity. Cell *141*, 315–330.

Zhu, A., Lee, D., and Shim, H. (2011). Metabolic positron emission tomography imaging in cancer detection and therapy response. Semin. Oncol. *38*, 55–69.

Journal of proteome research

ARTICLE

pubs.acs.org/jpr

# Proteome-wide Identification of Ubiquitylation Sites by Conjugation of Engineered Lysine-less Ubiquitin

Kiyotaka Oshikawa, Masaki Matsumoto, Koji Oyamada, and Keiichi I. Nakayama*

Department of Molecular and Cellular Biology, Medical Institute of Bioregulation, Kyushu University, 3-1-1 Maidashi, Higashi-ku, Fukuoka, Fukuoka 812-8582, Japan, and CREST, Japan Science and Technology Agency (JST), Kawaguchi, Saitama 332-0012, Japan

Supporting Information

ABSTRACT: Ubiquitin conjugation (ubiquitylation) plays important roles not only in protein degradation but also in many other cellular functions. However, the sites of proteins that are targeted for such modification have remained poorly characterized at the proteomic level. We have now developed a method for the efficient identification of ubiquitylation sites in target proteins with the use of an engineered form of ubiquitin (K0-Ub), in which all seven lysine residues are replaced with arginine. K0-Ub is covalently attached to lysine residues of target proteins via an isopeptide bond, but further formation of a polyubiquitin chain does not occur on K0-Ub. We identified a total of 1392 ubiquitylation sites of 794 proteins from HEK293T cells. Profiling of ubiquitylation sites indicated that the sequences surrounding lysine residues targeted for ubiquitin conjugation do not share a common motif or structural feature. Furthermore, we identified a critical ubiquitylation site of the cyclin-dependent kinase inhibitor $p27^{Kip1}$. Mutation of this site thus inhibited ubiquitylation of and stabilized $p27^{Kip1}$, suggesting that this lysine residue is the target site of $p27^{Kip1}$ for ubiquitin conjugation in vivo. In conclusion, our method based on K0-Ub is a powerful tool for proteome-wide identification of ubiquitylation sites of target proteins.

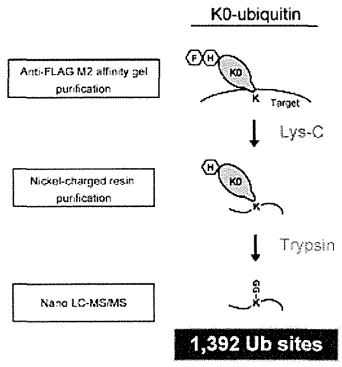


KEYWORDS: ubiquitylation, posttranslational modification, ubiquitin profiling, lysine-less ubiquitin, mass spectrometry, $p27^{Kip1}$

## INTRODUCTION

Conjugation of ubiquitin (ubiquitylation) to protein substrates plays an integral role in regulation of diverse physiological processes and in maintenance of cellular homeostasis in eukaryotes.[1−3] Ubiquitin is a highly conserved protein of 76 amino acids and is covalently conjugated to substrates by a cascade of reactions catalyzed by a ubiquitin-activating enzyme (E1), a ubiquitin-conjugating enzyme (E2), and a ubiquitin-protein isopeptide ligase (E3).[4] The COOH-terminal glycine residue of ubiquitin is covalently linked through an isopeptide bond to the ε-amino group of a lysine residue (or residues) in the substrate. It is likely that many thousands of human proteins are ubiquitylated in vivo in a highly regulated and spatiotemporal-dependent manner.

Recent technological advances in mass spectrometry (MS)-based protein identification have made it possible to detect various types of posttranslational modifications.[5−7] In the case of ubiquitylation, trypsin digestion of a ubiquitin-conjugated protein yields a "ubiquitin signature peptide," in which tandem glycine residues derived from the COOH-terminus of ubiquitin are conjugated at the lysine residue of the substrate.[8,9] Conjugation of ubiquitin to the lysine residue gives rise to a mass shift (+114.0429 Da) and miscleavage by trypsin, resulting in the generation of a T-shaped peptide.[10] On the basis of these characteristics, ubiquitin modification sites are identified as unique tandem MS (MS/MS) spectra in database searches. Approaches to the comprehensive identification of protein ubiquitylation sites have included those based on the use of (i) affinity-tagged ubiquitin,[9,11−14] (ii) antibodies to (anti-) ubiquitin,[15−18] (iii) ubiquitin-binding proteins,[11,19−21] and (iv) antibodies specific for the ubiquitin remnant.[22] However, large-scale identification of ubiquitylated sites has been unsuccessful, because ubiquitin forms polyubiquitin chains that are heterogeneous in length and in topology, making it difficult to identify ubiquitylated sites of target proteins. Moreover, many ubiquitylated proteins undergo degradation by the ubiquitin−proteasome system; the turnover of these unstable intermediates is rapid, with the result that their steady-state levels are low. Despite the biological and clinical importance of ubiquitylation, our knowledge of ubiquitylated proteins and their modification sites thus remains limited. An effective method to enrich ubiquitin-conjugated proteins and to identify the ubiquitylation sites therefore remains highly desirable.

Many groups including ours have attempted to develop MS-based approaches to the comprehensive identification of ubiquitylation sites. Peng et al. identified 110 ubiquitylation sites in yeast with the use of hexahistidine ($His_6$)-tagged ubiquitin.[9] Recent development of anti-diglycine markedly improved the efficiency of identification of ubiquitylation sites, but it has still been difficult to identify >1000 ubiquitylation sites at a time. Furthermore, the anti-diglycine method is unable to discriminate ubiquitylation from other modifications such as conjugation with the ubiquitin-like protein Nedd8 (neddylation).[22]

We have now developed an effective method for the identification of ubiquitylation sites based on an engineered lysine-less

Received: July 16, 2011
Published: November 05, 2011

form of ubiquitin (K0-Ub), and with this approach we have determined 1392 ubiquitylation sites of proteins from HEK293T cells. Wild-type ubiquitin (WT-Ub) contains seven lysine residues, all of which can be used for the formation of diverse ubiquitin chain linkages. Whereas K0-Ub is unable to form ubiquitin chains because of the lack of the ε-amino group of lysine, it can be linked to lysine residues of target proteins via an isopeptide bond. Two-step digestion of K0-Ub-modified proteins with lysyl endopeptidase (Lys-C) and trypsin coupled with affinity purification allowed us to efficiently enrich the ubiquitin signature peptides derived from target proteins. This method thus allows the large-scale and precise identification of ubiquitylation sites. Our results also provide insight into the characteristics of ubiquitylation sites, and we validated the approach by analysis of cyclin-dependent kinase (CDK) inhibitor $p27^{Kip1}$.

## METHODS

### Reagents

Ubiquitin aldehyde (Ub-CHO), leupeptin, and MG132 were obtained from Peptide Institute (Osaka, Japan). Iodoacetamide (IAA), aprotinin, and phenylmethylsulfonyl fluoride (PMSF) were from Wako (Osaka, Japan). Thymidine, cycloheximide (CHX), and other reagents, unless indicated otherwise, were obtained from Sigma (St. Louis, MO).

### Antibodies

Antibodies to ubiquitin were obtained from Abcam (Cambridge, United Kingdom); those to the FLAG epitope (M2) were from Sigma; those to cyclin D1 and to glutathione *S*-transferase (GST) were from MBL (Nagoya, Japan); those to $p27^{Kip1}$ and to HSP90 were from BD Biosciences (San Jose, CA); and those to the hemagglutinin epitope (HA11) were from Covance (Princeton, NJ).

### Cell Culture and Transfection

Human embryonic kidney 293T (HEK293T) and HeLa cells were cultured under an atmosphere of 5% $CO_2$ at 37 °C in Dulbecco's modified Eagle's medium (DMEM, Invitrogen, Carlsbad, CA) supplemented with 10% fetal bovine serum (Invitrogen). Cell transfection was performed with the use of the FuGENE 6 reagent (Roche, Indianapolis, IN).

### Immunoblot Analysis

Cell lysis and immunoblot analysis were performed as described.[23] Briefly, cells were lysed in buffer containing 50 mM Tris-HCl (pH 7.5), 300 mM NaCl, 0.5% Triton X-100, aprotinin (10 μg/mL), leupeptin (10 μg/mL), 1 mM PMSF, 0.4 mM $Na_3VO_4$, 0.4 mM EDTA, 10 mM NaF, and 10 mM sodium pyrophosphate. The lysate was centrifuged at 20000*g* for 15 min at 4 °C, and the resulting supernatant was separated by SDS–polyacrylamide gel electrophoresis (PAGE), transferred to a Immobilon-P membrane (Millipore, Billerica, MA), and subjected to immunoblot analysis. Immune complexes were detected with Supersignal West Pico chemiluminescence reagent (Pierce, Waltham, MA).

### Preparation of Ubiquitin Signature Peptides

The cDNAs encoding FLAG- and $His_6$-tagged WT-Ub or K0-Ub were subcloned into the pcDNA3 mammalian expression plasmid (Invitrogen). Transfected HEK293T cells from 10 15-cm Petri dishes were harvested, washed twice with ice-cold phosphate-buffered saline, and lysed in 20 mL of buffer A [50 mM Tris-HCl (pH 7.5), 300 mM NaCl, 0.5% Triton X-100, 25 mM IAA, aprotinin (10 μg/mL), leupeptin (20 μg/mL), 1 mM PMSF, 0.4 mM $Na_3VO_4$, 0.4 mM EDTA, 10 mM NaF, 10 mM sodium pyrophosphate]. The lysate was centrifuged at 20 000*g* for 15 min at 4 °C, and the resulting supernatant was mixed with anti-FLAG M2 affinity gel (500 μL, Sigma) with rotation for 30 min at 4 °C. The affinity gel was then washed with buffer B [25 mM Tris-HCl (pH 7.5), 150 mM NaCl, 0.25% Triton X-100, 1 mM PMSF, 0.4 mM $Na_3VO_4$, 0.4 mM EDTA, 10 mM NaF, 10 mM sodium pyrophosphate] and subjected to elution with 2 mL of the FLAG peptide (0.5 mg/mL, Sigma) in buffer B. Proteins in the eluate were denatured with 8 M urea, after which the sample was diluted to 4 M urea and Lys-C (1:100 w/w, Wako) was added. The digested sample (4 mL) was mixed with 50 μL of nickel-charged resin (ProBond resin, Invitrogen) by rotation for 1 h at 4 °C, after which the resin was washed with buffer C [25 mM Tris-HCl (pH 7.5), 150 mM NaCl, 100 mM imidazole, 50% acetonitrile] and then suspended directly in SDS sample buffer. The $His_6$-K0-Ub conjugates were separated by SDS–PAGE on a 15% gel and stained with Coomassie brilliant blue G-250. Gel pieces containing the stained proteins were treated first with 10 mM dithiothreitol at 56 °C for 45 min and then with 55 mM IAA at 25 °C for 30 min. In-gel digestion by trypsin (Promega, Madison, WI) and peptide extraction were performed as described.[24] The samples were then desalted with the use of StageTips with C18 Empore disk membranes (3M, St. Paul, MN).[25]

### MS Analysis and Database Search

The obtained peptides were dried and then dissolved in a solution containing 0.1% trifluoroacetic acid and 2% acetonitrile before nanoscale liquid chromatography (nanoLC)–MS/MS analysis with a system consisting of an LTQ Orbitrap Velos mass spectrometer (Thermo Fisher Scientific, Waltham, MA) coupled with a nanoLC instrument (Advance, Michrom BioResources, Auburn, CA) and HTC-PAL autosampler (CTC Analytics, Zwingen, Switzerland). Peptide separation was performed with an in-house pulled fused silica capillary (internal diameter, 0.1 mm; length, 15 cm; tip internal diameter, 0.05 mm) packed with 3-μm $C_{18}$ L-column (Chemicals Evaluation and Research Institute, Japan). The mobile phases consisted of 0.1% formic acid (A) and 100% acetonitrile (B). Peptides were eluted with a gradient of 5–35% B for 180 min at a flow rate of 200 nL/min. Collision-induced dissociation (CID) spectra were acquired automatically in the data-dependent scan mode with the dynamic exclusion option. Full MS spectra were obtained with Orbitrap in the mass/charge ($m/z$) range of 300–2000 with a resolution of 30 000. The nine most intense precursor ions in the full MS spectra were selected for subsequent ion-trap MS/MS analysis with the automated gain control mode. Lock mass function was activated to minimize mass error during analysis. The peak lists were generated by MSn.exe (Thermo Fisher Scientific) with a minimum scan/group value of 1 and were compared with in-house-curated target/decoy Human International Protein Index version 3.16 database (IPI, 57 366 protein sequences; European Bioinformatics Institute) with the use of the MASCOT algorithm (ver. 2.1.4). Trypsin was selected as the enzyme used, the allowed number of missed cleavages was set at 2, and carbamidomethylation on cysteine was selected as the fixed modification. Oxidized methionine, $NH_2$-pyroglutamine, lysine modified with diglycine, and protein modified with diglycine at its $NH_2$-terminus were searched as variable modifications. Precursor mass tolerance was 10 ppm, and tolerance of MS/MS ions was 0.5 Da. The threshold used for peptide identification was a MASCOT

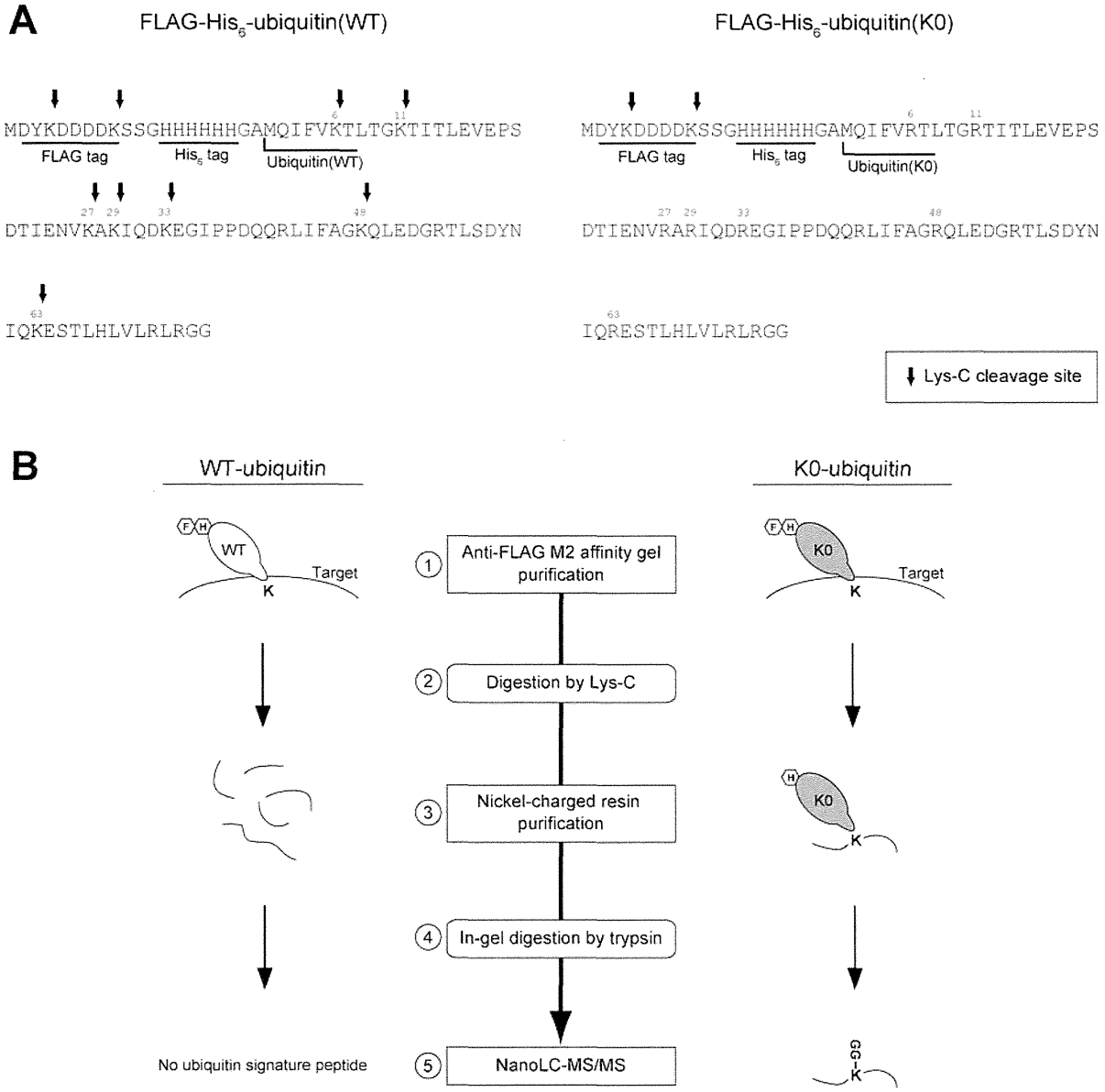


**Figure 1.** Strategy to identify ubiquitylation sites with K0-Ub. (A) Amino acid sequences of wild-type ubiquitin (WT-Ub) and lysine-less mutant ubiquitin (K0-Ub) tagged with tandem FLAG and $His_6$ epitopes. Arrows indicate the positions of potential Lys-C cleavage sites. (B) Cells are transfected with plasmids for expression of either WT-Ub (control) or K0-Ub tagged with the FLAG-$His_6$ tandem epitopes. The cells are then lysed, and ubiquitylated proteins are purified with an anti-FLAG column. Enriched ubiquitylated proteins are digested with Lys-C under denaturing conditions. WT-Ub is digested by Lys-C, and so no ubiquitin signature peptides should be recovered. On the other hand, Lys-C-resistant K0-Ub and its conjugated target protein fragments are further purified with nickel-charged resin. Enriched K0-Ub conjugates are separated by SDS-PAGE, subjected to in-gel digestion with trypsin, and analyzed by nanoLC-MS/MS.

score of ≥30 and a delta score (the difference between first-assigned and second-assigned peptides) of ≥18. With these criteria, the false positive rate was <1%.

### Identification of Abundant Proteins with emPAI

To compare ubiquitylated proteins identified in the study with abundant proteins of HEK293T cells, we constructed an abundant protein list with the use of the exponentially modified protein abundance index (emPAI). HEK293T cells were lysed in a solution containing 50 mM Tris-HCl (pH 7.5), 300 mM NaCl, 0.5% Triton X-100, aprotinin (10 μg/mL), leupeptin (20 μg/mL), 1 mM PMSF, 0.4 mM $Na_3VO_4$, 0.4 mM EDTA, 10 mM NaF, and 10 mM sodium pyrophosphate. The lysate was centrifuged at 20000*g* for 15 min at 4 °C, and proteins in the resulting supernatant were fractionated by SDS-PAGE on a 12% gel and stained with Coomassie brilliant blue G-250. Each lane of the gel was cut into 16 slices, which were treated first with 10 mM DTT at 56 °C for 45 min and then with 55 mM IAA at 25 °C for 30 min. In-gel digestion with trypsin and peptide extraction were performed, and the resulting peptides were analyzed by MS. With the use of a MASCOT database search, we counted the number of observed unique parent ions per protein. The emPAI value was calculated from the number of observed unique parent ions per protein and the number of observable peptides per protein. Ishihama et al.

previously defined emPAI and showed that it is directly proportional to protein content.[26,27]

### Bioinformatics Analysis

The sequences for 10 amino acids on each side of ubiquitylated lysines were extracted from the entire protein sequences. To compare the sequence logo around the identified ubiquitylation sites with the ~10 000 lysine residues randomly assigned from human IPI database version 3.16, we used WebLogo (http://weblogo.berkeley.edu).

To access the secondary structure types for ubiquitylated lysine residues, we searched for crystal structures of all the ubiquitylated proteins in the Protein Database Bank (PDB). A total of 151 PDB structures contained lysines that we found are susceptible to ubiquitylation (290 ubiquitylated lysines and 2463 total lysines). In cases where multiple PDB structures for a ubiquitylated protein were described, the structure of the best quality was used.

Subcellular localization of ubiquitylated proteins was analyzed and clustered with the use of the Gene Ontology (GO) term mapper after conversion of the Entrez Gene ID numbers of identified ubiquitylated proteins to UniProt Knowledgebase numbers by the UniProt ID mapping tool. A total of 1152 cellular components was found in the database, and the category was further grouped into five classes. Some proteins were predicted to have multiple subcellular localizations, whereas others had no subcellular information available in the database.

### Statistical Analysis

To determine whether the frequencies of ubiquitylation sites and ubiquitylated proteins were significantly higher than the frequencies of total lysine sites and proteins, we compared the frequencies using the normal approximation to the binomial distribution. A $p$ value of $<0.05$ was considered statistically significant.

### In Vitro Ubiquitylation Assay with Biotinylated K0-Ub

To prepare proteins modified with biotinylated ubiquitin, we subcloned the cDNA for WT-Ub or K0-Ub with an added $NH_2$-terminal cysteine residue as a biotinylation site into the pGEX-6P vector (GE Healthcare, Little Chalfont, United Kingdom). The encoded GST-tagged WT-Ub or K0-Ub proteins were expressed in *Escherichia coli* strain BL21(DE3) pLys(S) (Novagen, Darmstadt, Germany) cultured in the presence of 100 $\mu$M isopropyl-$\beta$-D-thiogalactopyranoside (IPTG). The bacterial cells were resuspended in 50 mM Tris-HCl (pH 7.5) containing 500 mM NaCl and then lysed by ultrasonic treatment (Branson Sonifier, Teltow, Germany). The lysate was centrifuged at 20 000$g$ for 10 min at 4 °C to remove debris, and the resulting supernatant was mixed with glutathione-Sepharose 4B (GE Healthcare) with rotation at 4 °C for 30 min. The beads were then washed with 50 mM Tris-HCl (pH 7.5) containing 500 mM NaCl, and the GST-tagged proteins were eluted with 50 mM Tris-HCl (pH 7.5) containing 10 mM reduced glutathione. The GST tag was cleaved from the isolated proteins with PreScission Protease (GE Healthcare). The purity of the recombinant proteins was confirmed by SDS-PAGE and staining with Coomassie brilliant blue G-250 (data not shown). The purified samples were biotinylated with the use of EZ-Link iodoacetyl-$PEO_2$-biotin (Pierce). To confirm the biotinylation, we measured the molecular mass of biotinylated WT-Ub and K0-Ub by MALDI-TOF MS analysis (data not shown).

Biotinylated WT-Ub or K0-Ub (500 ng) was incubated for various times at 30 °C in a final volume of 20 $\mu$L with E1 (100 ng, Boston Biochem, Cambridge, MA) and E2 (200 ng of UbcH5c[28] in the presence of an ATP-regenerating system [25 mM Tris-HCl (pH 7.5), 120 mM NaCl, 1 mM $MgCl_2$, 2 mM ATP, 1 mM creatine phosphate, phosphocreatine kinase (0.5 U/mL)]. The reaction was terminated by the addition of SDS sample buffer,

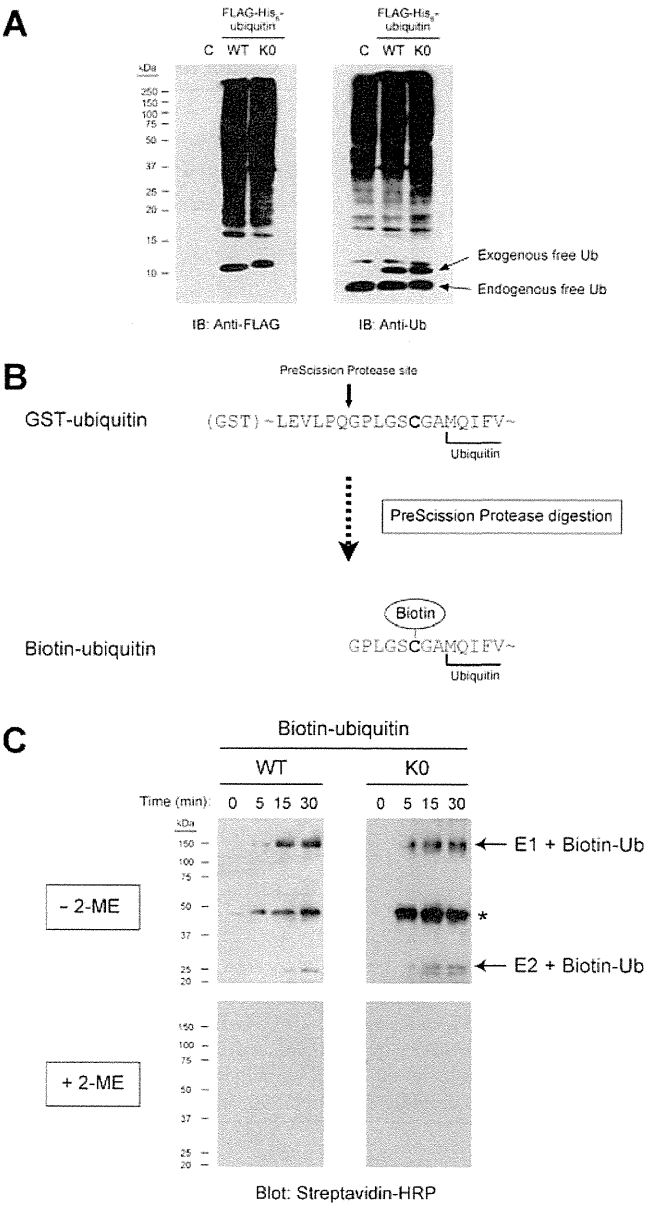


**Figure 2.** Effect of K0-Ub expression on cellular ubiquitylation. (A) HEK293T cells were transfected with plasmids encoding FLAG-$His_6$-tagged forms of WT-Ub or K0-Ub, or with the corresponding empty vector (C), after which cell lysates were subjected to immunoblot (IB) analysis with anti-FLAG and antiubiquitin. (B) Preparation of biotinylated ubiquitin. Ubiquitin fused with GST as well as an intervening PreScission Protease site and additional cysteine residue as a biotinylation target was expressed in *E. coli* and purified with glutathione–Sepharose 4B. The GST tag was cleaved with PreScission Protease, and the remaining protein was biotinylated with the use of EZ-Link iodoacetyl-$PEO_2$-biotin. (C) Biotinylated WT-Ub or K0-Ub was incubated with E1, E2, and an ATP-regenerating system for the indicated times, after which the reaction mixture was subjected to SDS-PAGE in the absence or presence of 2-ME followed by blot analysis with streptavidin-HRP. Asterisk indicates a nonspecific band.

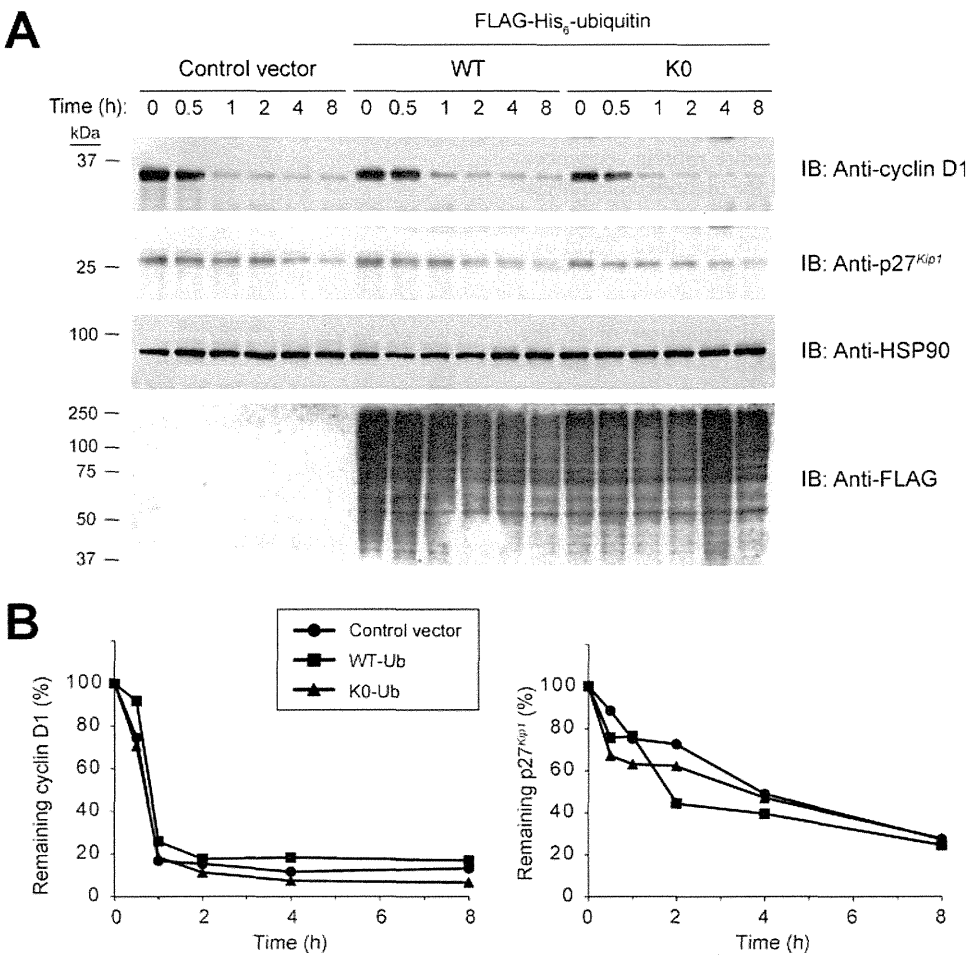


**Figure 3.** Effect of K0-Ub expression on the degradation of known ubiquitin—proteasome substrates. (A) The stability of endogenous cyclin D1 and $p27^{Kip1}$ in HEK293T cells expressing FLAG-$His_6$-tagged forms of WT-Ub or K0-Ub was monitored by incubation of the cells with CHX for the indicated times followed by immunoblot analysis with anti-cyclin D1 and anti-$p27^{Kip1}$. The blot was also probed with anti-HSP90 as a loading control and with anti-FLAG to reveal overall ubiquitylation. (B) The abundance of cyclin D1 or $p27^{Kip1}$ in the experiment shown in (A) was determined by densitometry, normalized by that of HSP90, and expressed relative to the value for time zero.

and each reaction mixture was subjected to SDS-PAGE on a 12% gel followed by blot analysis with a horseradish peroxidase (HRP)-streptavidin conjugate (SouthernBiotech, Birmingham, AL). To preserve thioester bonds in E1 and E2, we terminated the reaction under nonreducing conditions by using SDS sample buffer without 2-mercaptoethanol (2-ME).

### In Vitro Assay of $p27^{Kip1}$ Ubiquitylation

Human $p27^{Kip1}$ cDNA was subcloned into pGEX-6P for production of the GST-tagged protein in bacteria. The K165R mutant of $p27^{Kip1}$ was constructed by replacing the codon for $Lys^{165}$ with a codon for arginine by site-directed mutagenesis with the use of a QuickChange kit (Stratagene, La Jolla, CA). GST-tagged $p27^{Kip1}$ (WT or K165R) proteins were expressed in *E. coli* strain BL21 (DE3) pLys(S) cultured in the presence of 500 $\mu$M IPTG. The bacterial cells were resuspended in 50 mM Tris-HCl (pH 7.5) containing 500 mM NaCl and then lysed by ultrasonic treatment. The lysate was centrifuged at 20 000*g* for 10 min at 4 °C to remove debris, and the resulting supernatant was mixed with glutathione—Sepharose 4B with rotation at 4 °C for 30 min. The beads were then washed with 50 mM Tris-HCl (pH 7.5) containing 500 mM NaCl, and the GST-tagged proteins were eluted with 50 mM Tris-HCl (pH 7.5) containing 10 mM reduced glutathione. The purity of the recombinant proteins was confirmed by SDS-PAGE and staining with Coomassie brilliant blue G-250 (data not shown).

For in vitro assay of $p27^{Kip1}$ ubiquitylation, we prepared a ubiquitin ligase fraction from HEK293T cells. The cells were washed with phosphate-buffered saline, suspended in hypotonic buffer containing 20 mM Tris-HCl (pH 7.5), 10 mM KCl, 1.5 mM $MgCl_2$, and 250 mM sucrose, and subjected to three cycles of freezing and thawing. The resulting lysate was centrifuged at 100000*g* for 4 h at 4 °C, and the resulting supernatant (S100Pr−), from which proteasomes had been removed, was retrieved and frozen at −80 °C.

One microgram of GST-tagged $p27^{Kip1}$ (WT or K165R) was incubated for various times at 30 °C in a final volume of 20 $\mu$L with S100Pr− (8 $\mu$g), hemagglutinin epitope (HA)-tagged ubiquitin (0.5 $\mu$g),[28] Ub-CHO (100 $\mu$g/mL), 1 mM dithiothreitol, a protease inhibitor mixture (aprotinin, leupeptin, and PMSF each at 10 $\mu$g/mL), and a proteasome inhibitor (10 $\mu$M MG132) in the presence of an ATP-regenerating system [25 mM Tris-HCl (pH 7.5), 120 mM NaCl, 1 mM $MgCl_2$, 2 mM ATP, 1 mM creatine phosphate, phosphocreatine kinase (0.5 U/mL)].

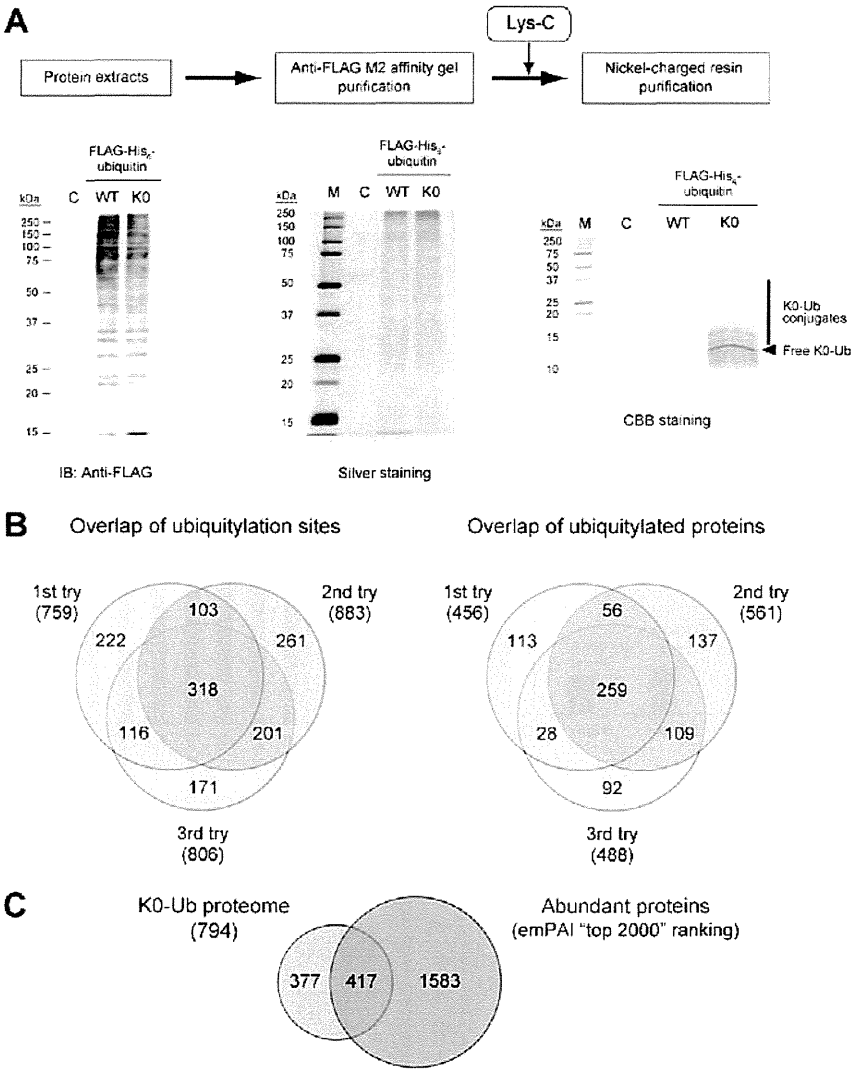


**Figure 4.** Overview of K0-Ub proteome analysis. (A) Protein extracts of HEK293T cells expressing FLAG-$His_6$-tagged WT-Ub or K0-Ub, or of cells transfected with the corresponding empty vector (C), were subjected to immunoblot analysis with anti-FLAG (left panel). The protein samples were subjected to purification with anti-FLAG M2 affinity gel and then analyzed by SDS-PAGE and silver staining (center panel; lane M, molecular size standards). After Lys-C treatment, which results in the digestion of WT-Ub conjugates but not that of K0-Ub conjugates, the protein samples were subjected to purification with nickel-charged resin followed by SDS-PAGE and staining with Coomassie brilliant blue G-250 (CBB) (right panel). (B) Venn diagrams showing overlap of K0-ubiquitylated sites and proteins in three independent experiments performed with HEK293T cells. (C) Venn diagram showing overlap of the K0-Ub proteome and abundant proteins (emPAI "top 2000" ranking) for HEK293T cells.

The reaction was terminated by the addition of SDS sample buffer, and each reaction mixture was subjected to SDS-PAGE on a 9% gel followed by immunoblot analysis with anti-GST.

### In Vivo Assay of $p27^{Kip1}$ Ubiquitylation

HeLa cells were synchronized at the $G_1$−S transition with a double thymidine block. Between the first (2 mM thymidine for 18 h) and second (2 mM thymidine for 16 h) blocks, the cells were transfected with pcDNA3 vectors for $His_6$-tagged ubiquitin and HA-$p27^{Kip1}$ (WT or K165R). Proteins conjugated with $His_6$-tagged ubiquitin were purified from the transfected cells with nickel-charged resin under denaturing conditions, fractionated by SDS-PAGE, and subjected to immunoblot analysis with anti-HA.

### Protein Degradation Analysis

HEK293T cells were transfected with pcDNA3 vectors for FLAG-$His_6$-tagged ubiquitin (WT-Ub or K0-Ub). For half-life studies, CHX (50 $\mu$g/mL) was added to the culture medium 24 h after transfection. At various times thereafter, the cells were lysed for measurement of endogenous protein abundance by immunoblot analysis.

Alternatively, HA-tagged human $p27^{Kip1}$ (WT or K165R) cDNA was subcloned into pcDNA3 for transfection of HEK293T cells. For half-life studies, CHX (50 $\mu$g/mL) was added to the medium 24 h after transfection. At various times thereafter, the cells were lysed and the abundance of HA-$p27^{Kip1}$ was measured by immunoblot analysis with anti-HA.

## RESULTS AND DISCUSSION

### Strategy for Identification of Ubiquitylation Sites

For comprehensive analysis of human ubiquitylated proteins, we have developed a new method for identification of ubiquitylation sites with the use of K0-Ub, in which all seven lysines of WT-Ub are replaced with arginine (Figure 1A). This method consists

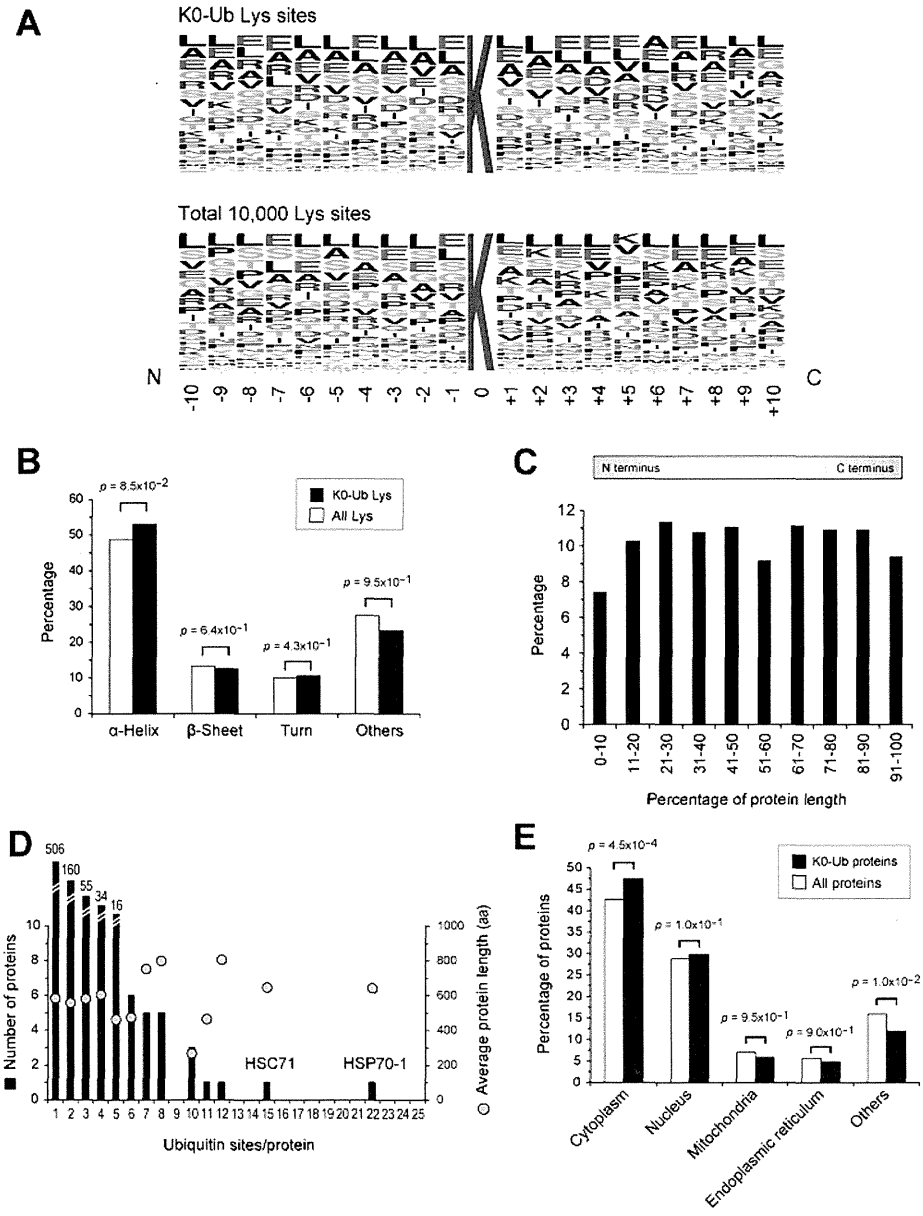


**Figure 5.** Properties of K0-ubiquitylated sites and proteins. (A) Sequence logo plots representing amino acid frequencies for ±10 amino acids relative to identified lysine ubiquitylation sites (upper panel). The sequence logo for 10 000 lysine residues randomly assigned from human IPI database version 3.16 is shown as a control (lower panel). (B) Distribution of secondary structures for all lysines and K0-ubiquitylated lysines obtained from an analysis of 151 PDB structures (290 K0-ubiquitylated lysines and 2463 total lysines). (C) Distribution of the 1392 identified ubiquitylation sites within their protein sequences. The length of each protein is normalized to 100%. (D) Number of ubiquitylation sites for the 794 identified ubiquitylated proteins. Average protein length in amino acids (aa) for proteins with the same number of ubiquitylation sites is indicated by circles. (E) Subcellular localization of all proteins and K0-ubiquitylated proteins determined by GO cellular component analysis.

of five steps: (i) affinity capture of proteins conjugated with FLAG- and $His_6$-tagged K0-Ub with anti-FLAG M2 affinity gel, (ii) digestion of the captured proteins with Lys-C, (iii) enrichment of peptides conjugated with K0-Ub with the use of nickel-charged resin, (iv) digestion of the peptides with trypsin, and (v) identification of ubiquitin signature peptides with nano-LC-MS/MS technology (Figure 1B). Given that neither K0-Ub nor the $His_6$ tags contain lysine residues and they are therefore resistant to digestion by Lys-C, peptides conjugated with $His_6$-K0-Ub are enriched by chromatography with nickel-charged resin. In contrast, peptides conjugated with $His_6$-WT-Ub are not recovered because WT-Ub undergoes multiple cleavages by Lys-C. The ubiquitin signature peptides are generated by in-gel tryptic digestion and identified by nanoLC-MS/MS.

### Effect of K0-Ub Expression on Cellular Ubiquitylation

Excessive expression of K0-Ub might be expected to inhibit elongation of polyubiquitin chains and protein turnover, potentially affecting a variety of cellular functions. We thus examined the level of K0-Ub expression in HEK293T cells transiently transfected with a vector for FLAG-$His_6$-tagged K0-Ub. Cell lysates were fractionated by SDS−PAGE and subjected to immunoblot analysis with anti-FLAG. The extent of polyubiquitin chain elongation did not appear to differ between cells expressing WT-Ub and


dx.doi.org/10.1021/pr200668y | J. Proteome Res. 2012, 11, 796–807

**Table 1. Identification by K0-Ub Proteome Analysis of Ubiquitylation Sites in Endogenous Ubiquitin**

| protein name (IPI accession number) | position | identified peptide sequence |
|---|---|---|
| UBIQUITIN (IPI00179330.6) | M1, K6: | M[a]QIFVK[a]TLTGKTITLEVEPSDTIENVK |
| | K6: | MQIFVK[a]TLTGK |
| | K6, K11: | MQIFVK[a]TLTGK[a]TITLEVEPSDTIENVK |
| | K11: | TLTGK[a]TITLEVEPSDTIENVK |
| | K11, K27: | TLTGK[a]TITLEVEPSDTIENVK[a]AK |
| | K27: | TITLEVEPSDTIENVK[a]AK |
| | K27, K29: | TITLEVEPSDTIENVK[a]AK[a]IQDK |
| | K33: | IQDK[a]EGIPPDQQR |
| | K48: | LIFAGK[a]QLEDGR |
| | K63: | TLSDYNIQK[a]ESTLHLVLR |

[a] Ubiquitin signature site.

those expressing K0-Ub (Figure 2A), suggesting that forced expression of K0-Ub did not substantially perturb cellular ubiquitylation.

We next estimated the ubiquitylation rate for K0-Ub in vitro. We produced biotinylated ubiquitin for an in vitro ubiquitylation assay (Figure 2B). Biotinylated ubiquitin (WT-Ub or K0-Ub) was then incubated with E1, E2 (UbcH5c), and an ATP-regenerating system, and the rates of E1 and E2 conjugation to biotinylated ubiquitin were measured. The conjugation of K0-Ub to E1 or E2, which was reversed in the presence of 2-ME, appeared almost identical to that of WT-Ub (Figure 2C). Together, these results suggested that K0-Ub is suitable for in vitro ubiquitylation and is efficiently attached to cellular target proteins in vivo.

To evaluate further the effect of K0-Ub expression on ubiquitin-dependent protein degradation, we investigated the degradation rates of two representative proteins, cyclin D1 and $p27^{Kip1}$, that are targeted by the ubiquitin–proteasome system. Cyclin D1 is a short-lived protein, with a half-life of <1 h. CHX chase experiments revealed that expression of K0-Ub did not affect the rate of cyclin D1 degradation (Figure 3). Likewise, overexpression of K0-Ub did not result in a delay in $p27^{Kip1}$ degradation (Figure 3). Although we were unable to detect the ubiquitylation of endogenous p27 probably due to its low abundance, these results suggested that the expression of K0-Ub in our system affects neither cellular ubiquitylation nor subsequent protein degradation by the ubiquitin–proteasome system, consistent with the results of a recent report by Ziv et al.[29]

## Comprehensive Identification of Protein Ubiquitylation Sites

With our new method, we next performed a comprehensive analysis to identify ubiquitylation sites of a large number of proteins in human cells. HEK293T cells were transfected with a vector encoding FLAG-$His_6$-tagged WT-Ub (control) or K0-Ub, and cell lysates were subjected to immunoblot analysis with anti-FLAG, revealing that the expression levels of WT-Ub and K0-Ub were similar (Figure 4A). The lysates were then subjected to purification with anti-FLAG M2 affinity gel followed by Lys-C digestion and purification with nickel-charged resin, and the resulting samples were fractionated by SDS-PAGE and stained with Coomassie brilliant blue G-250 (Figure 4A). The samples derived from cells expressing K0-Ub contained K0-Ub conjugates that migrated more slowly than did free K0-Ub, whereas no signal was visible with the samples derived from cells expressing WT-Ub. The purified peptides were further digested with trypsin and subjected to LC–MS/MS analysis.

We identified >750 ubiquitylation sites in a single analysis of HEK293T cells (Figure 4B). Three independent analyses resulted in the identification of 1392 ubiquitylation sites of 794 proteins, with the overall false discovery rate for peptides and proteins being <1% (Supplementary Tables S1 and S2, Supporting Information). The false discovery rate for ubiquitylated lysine–containing peptides, as opposed to all peptides, was even lower (0.3–0.4%).

We compared the identified ubiquitylated proteins with the abundant proteins of HEK293T cells ranked by the exponentially modified protein abundance index (emPAI "top 2000" ranking), which is calculated from the number of observed peptides per protein and the number of observable peptides per protein (Supplementary Table S3, Supporting Information). About half of the ubiquitylated proteins were not included among the "top 2000" abundant proteins (Figure 4C), suggesting that not only highly abundant proteins but also proteins of low abundance can be detected by our method. These results further suggest that the ubiquitinylated proteome differs from the total proteome.

## Bioinformatics Analysis of Ubiquitylated Sites and Proteins

To gain insight into how lysine ubiquitylation might be regulated at the level of primary structure, we analyzed our data for local sequence context by extracting a ±10-residue sequence window surrounding each ubiquitylation site (Figure 5A). We compared the sequence logo for the identified ubiquitylation sites to that for 10 000 randomly assigned lysine residues (Figure 5A). Overall, no significant sequence recognition motif was detected among the identified ubiquitylation sites, possibly because they reflect reactions catalyzed by numerous E3 ligases.[30] We next compared the secondary structures around ubiquitylated lysines to those around all lysines. Structural information was available in the Protein Data Bank (PDB) for 151 of the 794 ubiquitylated proteins identified in our study, with these 151 proteins containing 290 ubiquitylated lysines and 2463 lysines in total. There was no statistically significant difference between ubiquitylated lysines and all lysines in secondary structure groups (Figure 5B), suggesting that ubiquitylation does not show any preference for primary or secondary structures. We also examined the position and number of ubiquitylation sites within identified proteins. The ubiquitylation sites were found to be evenly distributed throughout the identified proteins, with no significant bias toward the $NH_2$- or COOH-terminus (Figure 5C).

**Table 2. Identification by K0-Ub Proteome Analysis of Ubiquitylation Sites of Proteins Related to Cell Cycle and DNA Damage and Repair**

| IPI accession number | protein name | position | identified peptide sequence |
|---|---|---|---|
| | Cell Cycle Related | | |
| IPI00026689.4 | CELL DIVISION CONTROL PROTEIN 2 HOMOLOGUE | K58: | EISLLK[a]ELR |
| | | K136: | DLKPQNLLIDDK[a]GTIK |
| | | K207: | K[a]PLFHGDSEIDQLFR |
| IPI00007811.1 | CELL DIVISION PROTEIN KINASE 4 | K211: | RK[a]PLFCGNSEADQLGK |
| IPI00023529.1 | CELL DIVISION PROTEIN KINASE 6 | K26: | ADQQYECVAEIGEGAYGK[a]VFK |
| IPI00025087.1 | CELLULAR TUMOR ANTIGEN P53 | K120: | LGFLHSGTAK[a]SVTCTYSPALNK |
| | | K321: | KK[a]PLDGEYFTLQIR |
| | | K357: | DAQAGK[a]EPGGSR |
| | | K370: | AHSSHLK[a]SK |
| IPI00006991.1 | CYCLIN-DEPENDENT KINASE INHIBITOR 1B ($p27^{Kip1}$) | K165: | RPATDDSSTQNK[a]R |
| IPI00184330.5 | DNA REPLICATION LICENSING FACTOR MCM2 | K591: | GVCLIDEFDK[a]MNDQDR |
| IPI00013214.1 | DNA REPLICATION LICENSING FACTOR MCM3 | K351: | GDINILLIGDPSVAK[a]SQLLR |
| | | K435: | VTIAK[a]AGIHAR |
| IPI00018349.5 | DNA REPLICATION LICENSING FACTOR MCM4 | K536: | GQYTSGK[a]GSSAVGLTAYVMK |
| | | K600: | SVLHEVMEQQTLSIAK[a]AGIICQLNAR |
| | | K628: | K[a]TTIENIQLPHTLLSR |
| IPI00031517.1 | DNA REPLICATION LICENSING FACTOR MCM6 | K313: | FGGK[a]ELRDEEQTAESIK |
| | | K422: | AVYTSGK[a]ASSAAGLTAAVVR |
| | | K517: | SLK[a]QNINLSAPIMSR |
| | | K611: | DGSGVTK[a]SSWR |
| IPI00299904.3 | DNA REPLICATION LICENSING FACTOR MCM7 | K145: | FELYFQGPSSNK[a]PR |
| | | K387: | GNINICLMGDPGVAK[a]SQLLSYIDR |
| | | K471: | TAIHEVMEQQTISIAK[a]AGILTTLNAR |
| | | K648: | DSLLGDK[a]GQTAR |
| IPI00026309.3 | GEMININ | K139: | ENK[a]ELAEVAEHVQYMAELIER |
| | DNA Damage and Repair | | |
| IPI00412298.3 | ATAXIA TELANGIECTASIA AND RAD3-RELATED PROTEIN | K1057: | ALHYLK[a]NETEIELGSLLR |
| IPI00178431.11 | ATP-DEPENDENT DNA HELICASE Q1 | K38: | QQELIQK[a]K |
| IPI00075081.1 | FANCONI ANEMIA GROUP D2 PROTEIN | K561: | K[a]QLSSTVFK |
| IPI00024579.1 | POSTREPLICATION REPAIR PROTEIN RAD18 | K186: | SVEEIAPDPSEAK[a]RPEPPSTSTLK |
| | | K197: | RPEPPSTSTLK[a]QVTK |
| | | K309: | SAAEIVQEIENIEK[a]TR |
| | | K462: | DLLEEEEAWEASHK[a]NDLQDTEISPR |
| | | K218: | VDCPVCGVNIPESHINK[a]HLDSCLSR |
| IPI00021700.3 | PROLIFERATING CELL NUCLEAR ANTIGEN | K80: | ILK[a]CAGNEDIITLR |
| | | K164: | DLSHIGDAVVISCAK[a]DGVK |
| | | K254: | YYLAPK[a]IEDEEGS |
| IPI00291939.1 | STRUCTURAL MAINTENANCE OF CHROMOSOME 1 | K1196: | EEFYTK[a]AESLIGVYPEQGDCVISK |
| IPI00008219.1 | UV EXCISION REPAIR PROTEIN RAD23 HOMOLOGUE A | K47: | DAFPVAGQK[a]LIYAGK |
| | | K53: | LIYAGK[a]ILSDDVPIR |
| | | K78: | NFVVVMVTK[a]TK |
| | | K122: | EDK[a]SPSEESAPTTSPESVSGSVPSSGSSGR |
| IPI00102997.1 | WERNER HELICASE-INTERACTING PROTEIN 1 | K457: | VLITENDVK[a]EGLQR |

[a] Ubiquitin signature site.

Our analysis indicated that 506 out of the 794 identified proteins contained only a single lysine conjugated with ubiquitin, whereas the remaining 288 proteins contained multiple lysines that underwent ubiquitylation (Figure 5D). HSP70-1 and HSC71 were found to be ubiquitylated on at least 22 and 15 lysines, respectively, although the biological relevance of such extensive ubiquitylation of a chaperone molecule remains unknown. In addition, there was no apparent correlation between the number of ubiquitylation sites and protein length (Figure 5D). We next analyzed the subcellular localization of identified proteins on the basis of the "cellular component" of Gene Ontology (GO) slim annotations. The frequency of cytoplasmic localization for ubiquitylated proteins was slightly greater than that for total proteins (Figure 5E).

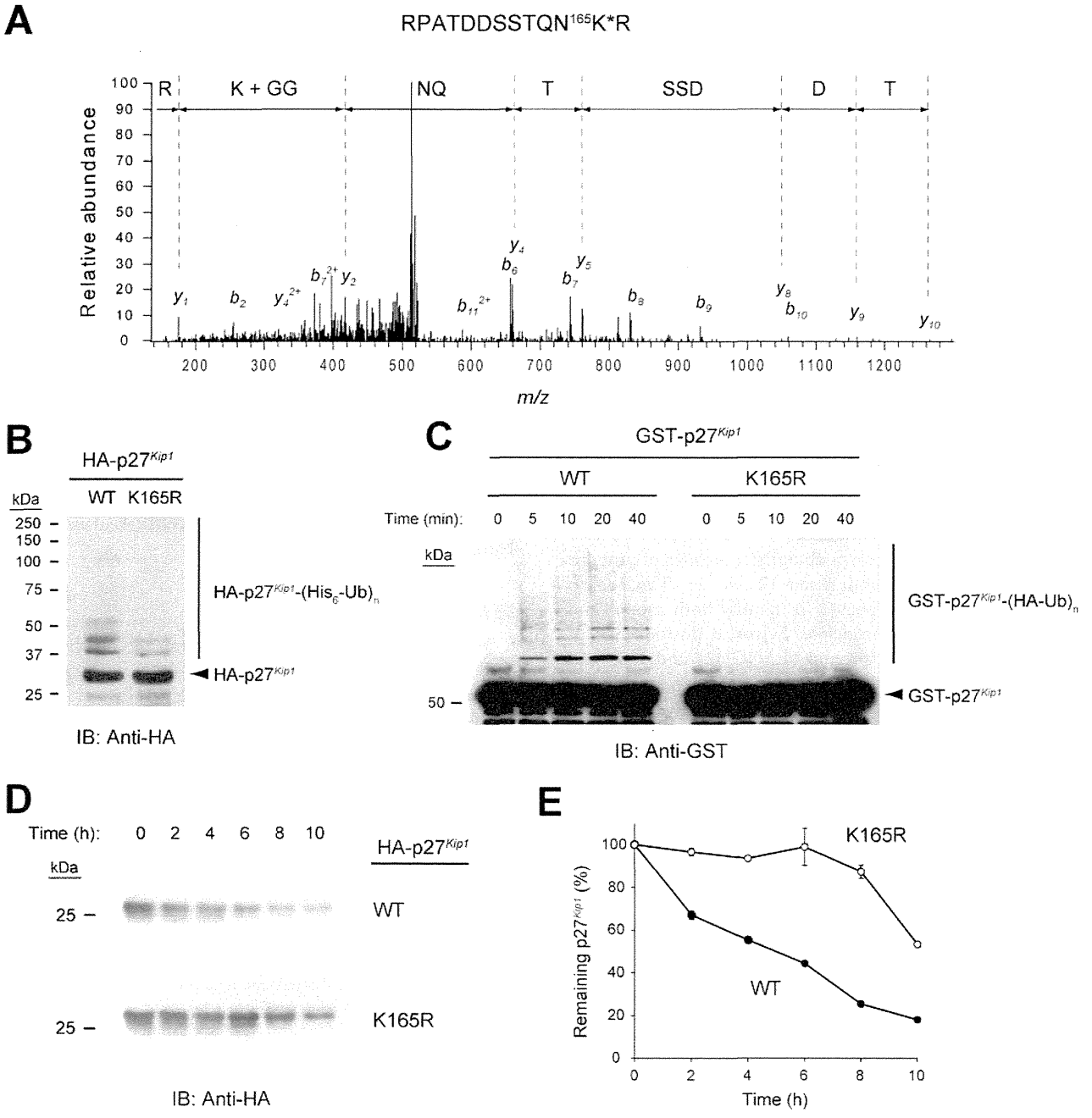


**Figure 6.** Lysine at position 165 is essential for ubiquitylation and degradation of $p27^{Kip1}$. (A) Our method identified $Lys^{165}$ of $p27^{Kip1}$ as a ubiquitylation site. The diglycine-modified lysine was detected by MS/MS analysis with CID fragmentation. (B) HeLa cells were synchronized at the $G_1$−S boundary of the cell cycle by double thymidine block. After the first block, the cells were transfected with vectors for $His_6$-tagged ubiquitin ($His_6$-Ub) and either wild-type or K165R mutant forms of HA-tagged $p27^{Kip1}$. After the second block, proteins conjugated with $His_6$-Ub were purified under denaturing conditions and subjected to immunoblot analysis with anti-HA. The arrowhead indicates the position of unmodified HA-$p27^{Kip1}$. (C) Recombinant GST-tagged wild-type or K165R mutant forms of $p27^{Kip1}$ were incubated for the indicated times with a fraction of HEK293T cell extract from which proteasomes had been removed by ultracentrifugation (S100Pr−) as well as with an ATP-regenerating system, as described in the Methods section. The reaction mixtures were subjected to immunoblot analysis with anti-GST. The arrowhead indicates the position of unmodified GST-$p27^{Kip1}$. (D) The stability of HA-$p27^{Kip1}$ (WT or K165R) was monitored by treatment of transfected HEK293T cells with CHX for the indicated times followed by immunoblot analysis with anti-HA. (E) The band intensity corresponding to HA-$p27^{Kip1}$ (WT or K165R) in experiments similar to that in (D) was normalized by that of HSP90 and then expressed relative to the corresponding value for time zero. Data are means ± SEM for three independent experiments.

The identified ubiquitylated proteins include proteins that have previously been shown to be ubiquitylated such as histones H2A and H2B, β-catenin, hypoxia-inducible factor 1α (HIF1α), Bax, signal transducer and activator of transcription 5a (STAT5a), and ubiquitin itself. In addition to the ubiquitylation of all seven lysines of ubiquitin, we also detected ubiquitylation of the $NH_2$-terminal methionine of endogenous ubiquitin (Table 1), which participates in the formation of linear ubiquitin chains.[31,32]

Many important regulators of cell cycle progression were also found to be ubiquitylated in our analysis (Table 2). For example, CDK1 (also known as CDC2), CDK4, and CDK6 were ubiquitylated, as was the CDK inhibitor $p27^{Kip1}$. Of note, five of six MCM proteins (MCM2, -3, -4, -6, and -7), which form a complex to serve as the major replicative helicase and the licensing factor for DNA replication, were found to be ubiquitylated, some of them extensively so. Geminin, an inhibitor of DNA replication licensing factor Cdt1, was also included in the list. Although degradation of CDKs and CDK inhibitors, as well as that of MCM proteins and geminin, is thought to occur during different phases of the cell cycle, these proteins were simultaneously identified, probably because we used asynchronous cells for our analysis. The tumor suppressor p53 was also found to be ubiquitylated on lysines 120, 321, 357, and 370. Lysine at position 120 was previously shown to undergo acetylation but not ubiquitylation,[33,34] but our results now show that it is indeed ubiquitylated. Lysines are often targeted by protein modifications such as acetylation, methylation, ubiquitylation, SUMOylation, and neddylation.[35−42] Whereas these modifications have their own specific roles, one modification can competitively inhibit another and its associated function.[43−47] Our data set also contains many previously known ubiquitylation sites of proteins related to DNA damage and repair (Table 2). The K0-Ub conjugation system was expected to identify both mono- and polyubiquitylation sites in principle. Lysine at position 561 of Fanconi anemia group D2 protein (FANCD2) and $Lys^{164}$ of proliferating cell nuclear antigen (PCNA), which have previously been identified as mono-ubiquitylation sites, were indeed detected by our method. We also identified a large number of novel ubiquitylation sites located on various proteins (Supplementary Table S2, Supporting Information).

### Validation Study for Ubiquitylation of $p27^{Kip1}$ on $Lys^{165}$

To validate our MS data set, we evaluated the cellular function of an identified ubiquitylation site of the CDK inhibitor $p27^{Kip1}$, which is rapidly degraded by the ubiquitin−proteasome system at the $G_1$−S transition of the cell cycle in response to mitogenic signals.[48,49] Our MS data set contains a unique site ($Lys^{165}$) for ubiquitylation of $p27^{Kip1}$ (Figure 6A). We previously showed that the extent of $p27^{Kip1}$ ubiquitylation was markedly reduced when lysine residues at positions 134, 153, and 165 were all replaced with arginine, suggesting that one or more of these lysine residues is the target for ubiquitin conjugation.[50] We therefore replaced $Lys^{165}$ of $p27^{Kip1}$ with arginine (K165R) and subjected the mutant protein to in vivo and in vitro ubiquitylation assays. These assays revealed that the level of ubiquitylation of the K165R mutant was greatly reduced compared with that of wild-type $p27^{Kip1}$ (Figure 6B,C). CHX chase analysis also showed that the K165R mutant was markedly more stable than wild-type $p27^{Kip1}$ (Figure 6D,E). This lysine residue therefore appears to be solely (or at least, largely) responsible for the degradation of $p27^{Kip1}$. We thus propose that our method can be applied to the identification of physiological ubiquitylation sites in a large number of proteins.

## CONCLUSIONS

Although lysine ubiquitylation has been studied extensively over the past 30 years, only a limited number of ubiquitylation sites have been identified to date, and important questions regarding the entire ubiquitin system still remain unanswered. We have now established a method for the large-scale identification of ubiquitylation sites based on K0-Ub, and we have shown that this approach is able to identify in vivo ubiquitylation sites of ubiquitin−proteasome target proteins. Engineered ubiquitin (K0-Ub) is thus a powerful tool to identify biological ubiquitylation reactions. We have identified 1392 sites in 794 proteins in the present study. In conclusion, our data provide extensive insight into human ubiquitylation sites, together with novel information regarding the nature of ubiquitylation.

## ASSOCIATED CONTENT

### Supporting Information

The detailed information of identified peptides and proteins are listed in Supplementary Tables S1 and S2. The emPAI value of "top 2000" proteins from HEK293T cells are listed in Supplementary Table S3. This material is available free of charge via the Internet at http://pubs.acs.org.

## AUTHOR INFORMATION

### Corresponding Author

*Tel.: +81-92-642-6815. Fax: +81-92-642-6819. E-mail: nakayak1@bioreg.kyushu-u.ac.jp.

## ACKNOWLEDGMENT

We thank M. Oda, E. Koba, T. Takami, and N. Nishimura for technical assistance, and A. Ohta for help in preparation of the manuscript. This work was supported in part by a grant from the Ministry of Education, Culture, Sports, Science, and Technology of Japan.

## REFERENCES

(1) Hershko, A.; Ciechanover, A. The ubiquitin system. *Annu. Rev. Biochem.* **1998**, *67*, 425–479.

(2) Pickart, C. M. Mechanisms underlying ubiquitination. *Annu. Rev. Biochem.* **2001**, *70*, 503–533.

(3) Finley, D.; Ciechanover, A.; Varshavsky, A. Ubiquitin as a central cellular regulator. *Cell* **2004**, *116* (2 Suppl), S29–S322 p following S.

(4) Scheffner, M.; Nuber, U.; Huibregtse, J. M. Protein ubiquitination involving an E1-E2-E3 enzyme ubiquitin thioester cascade. *Nature* **1995**, *373* (6509), 81–83.

(5) Aebersold, R.; Mann, M. Mass spectrometry-based proteomics. *Nature* **2003**, *422* (6928), 198–207.

(6) Witze, E. S.; Old, W. M.; Resing, K. A.; Ahn, N. G. Mapping protein post-translational modifications with mass spectrometry. *Nat. Methods* **2007**, *4* (10), 798–806.

(7) Choudhary, C.; Mann, M. Decoding signalling networks by mass spectrometry-based proteomics. *Nat. Rev. Mol. Cell. Biol.* **2010**, *11* (6), 427–439.

(8) Marotti, L. A., Jr.; Newitt, R.; Wang, Y.; Aebersold, R.; Dohlman, H. G. Direct identification of a G protein ubiquitination site by mass spectrometry. *Biochemistry* **2002**, *41* (16), 5067–5074.

(9) Peng, J.; Schwartz, D.; Elias, J. E.; Thoreen, C. C.; Cheng, D.; Marsischky, G.; Roelofs, J.; Finley, D.; Gygi, S. P. A proteomics approach to understanding protein ubiquitination. *Nat. Biotechnol.* **2003**, *21* (8), 921–926.

(10) Xu, P.; Peng, J. Dissecting the ubiquitin pathway by mass spectrometry. *Biochim. Biophys. Acta* **2006**, *1764* (12), 1940–1947.

(11) Mayor, T.; Lipford, J. R.; Graumann, J.; Smith, G. T.; Deshaies, R. J. Analysis of polyubiquitin conjugates reveals that the Rpn10 substrate receptor contributes to the turnover of multiple proteasome targets. *Mol. Cell. Proteomics* **2005**, *4* (6), 741–751.

(12) Tagwerker, C.; Flick, K.; Cui, M.; Guerrero, C.; Dou, Y.; Auer, B.; Baldi, P.; Huang, L.; Kaiser, P. A tandem affinity tag for two-step

purification under fully denaturing conditions: application in ubiquitin profiling and protein complex identification combined with in vivocross-linking. *Mol. Cell. Proteomics* **2006**, *5* (4), 737–748.

(13) Meierhofer, D.; Wang, X.; Huang, L.; Kaiser, P. Quantitative analysis of global ubiquitination in HeLa cells by mass spectrometry. *J. Proteome Res.* **2008**, *7* (10), 4566–4576.

(14) Danielsen, J. M.; Sylvestersen, K. B.; Bekker-Jensen, S.; Szklarczyk, D.; Poulsen, J. W.; Horn, H.; Jensen, L. J.; Mailand, N.; Nielsen, M. L. Mass spectrometric analysis of lysine ubiquitylation reveals promiscuity at site level. *Mol. Cell. Proteomics* **2011**, *10* (3), M110 003590.

(15) Matsumoto, M.; Hatakeyama, S.; Oyamada, K.; Oda, Y.; Nishimura, T.; Nakayama, K. I. Large-scale analysis of the human ubiquitin-related proteome. *Proteomics* **2005**, *5* (16), 4145–4151.

(16) Vasilescu, J.; Smith, J. C.; Ethier, M.; Figeys, D. Proteomic analysis of ubiquitinated proteins from human MCF-7 breast cancer cells by immunoaffinity purification and mass spectrometry. *J. Proteome Res.* **2005**, *4* (6), 2192–2200.

(17) Newton, K.; Matsumoto, M. L.; Wertz, I. E.; Kirkpatrick, D. S.; Lill, J. R.; Tan, J.; Dugger, D.; Gordon, N.; Sidhu, S. S.; Fellouse, F. A.; Komuves, L.; French, D. M.; Ferrando, R. E.; Lam, C.; Compaan, D.; Yu, C.; Bosanac, I.; Hymowitz, S. G.; Kelley, R. F.; Dixit, V. M. Ubiquitin chain editing revealed by polyubiquitin linkage-specific antibodies. *Cell* **2008**, *134* (4), 668–678.

(18) Matsumoto, M. L.; Wickliffe, K. E.; Dong, K. C.; Yu, C.; Bosanac, I.; Bustos, D.; Phu, L.; Kirkpatrick, D. S.; Hymowitz, S. G.; Rape, M.; Kelley, R. F.; Dixit, V. M. K11-linked polyubiquitination in cell cycle control revealed by a K11 linkage-specific antibody. *Mol. Cell* **2010**, *39* (3), 477–484.

(19) Tan, F.; Lu, L.; Cai, Y.; Wang, J.; Xie, Y.; Wang, L.; Gong, Y.; Xu, B. E.; Wu, J.; Luo, Y.; Qiang, B.; Yuan, J.; Sun, X.; Peng, X. Proteomic analysis of ubiquitinated proteins in normal hepatocyte cell line Chang liver cells. *Proteomics* **2008**, *8* (14), 2885–96.

(20) Hjerpe, R.; Aillet, F.; Lopitz-Otsoa, F.; Lang, V.; England, P.; Rodriguez, M. S. Efficient protection and isolation of ubiquitylated proteins using tandem ubiquitin-binding entities. *EMBO Rep.* **2009**, *10* (11), 1250–1258.

(21) Shi, Y.; Chan, D. W.; Jung, S. Y.; Malovannaya, A.; Wang, Y.; Qin, J. A data set of human endogenous protein ubiquitination sites. *Mol. Cell. Proteomics* **2011**, *10* (5), M110002089.

(22) Xu, G.; Paige, J. S.; Jaffrey, S. R. Global analysis of lysine ubiquitination by ubiquitin remnant immunoaffinity profiling. *Nat. Biotechnol.* **2010**, *28* (8), 868–873.

(23) Nishiyama, M.; Oshikawa, K.; Tsukada, Y.; Nakagawa, T.; Iemura, S.; Natsume, T.; Fan, Y.; Kikuchi, A.; Skoultchi, A. I.; Nakayama, K. I. CHD8 suppresses p53-mediated apoptosis through histone H1 recruitment during early embryogenesis. *Nat. Cell Biol.* **2009**, *11* (2), 172–182.

(24) Oshikawa, K.; Matsumoto, M.; Yada, M.; Kamura, T.; Hatakeyama, S.; Nakayama, K. I. Preferential interaction of TIP120A with Cul1 that is not modified by NEDD8 and not associated with Skp1. *Biochem. Biophys. Res. Commun.* **2003**, *303* (4), 1209–1216.

(25) Rappsilber, J.; Mann, M.; Ishihama, Y. Protocol for micro-purification, enrichment, pre-fractionation and storage of peptides for proteomics using StageTips. *Nat. Protoc.* **2007**, *2* (8), 1896–1906.

(26) Ishihama, Y.; Oda, Y.; Tabata, T.; Sato, T.; Nagasu, T.; Rappsilber, J.; Mann, M. Exponentially modified protein abundance index (emPAI) for estimation of absolute protein amount in proteomics by the number of sequenced peptides per protein. *Mol. Cell. Proteomics* **2005**, *4* (9), 1265–1272.

(27) Shinoda, K.; Tomita, M.; Ishihama, Y. emPAI Calc--for the estimation of protein abundance from large-scale identification data by liquid chromatography-tandem mass spectrometry. *Bioinformatics* **2010**, *26* (4), 576–577.

(28) Hatakeyama, S.; Yada, M.; Matsumoto, M.; Ishida, N.; Nakayama, K. I. U box proteins as a new family of ubiquitin-protein ligases. *J. Biol. Chem.* **2001**, *276* (35), 33111–33120.

(29) Ziv, I.; Matiuhin, Y.; Kirkpatrick, D. S.; Erpapazoglou, Z.; Leon, S.; Pantazopoulou, M.; Kim, W.; Gygi, S. P.; Haguenauer-Tsapis, R.; Reis, N.; Glickman, M. H.; Kleifeld, O. A perturbed ubiquitin landscape distinguishes between ubiquitin in trafficking and in proteolysis. *Mol. Cell. Proteomics* **2011**, *10* (5), M111009753.

(30) Semple, C. A. The comparative proteomics of ubiquitination in mouse. *Genome Res.* **2003**, *13* (6B), 1389–1394.

(31) Kirisako, T.; Kamei, K.; Murata, S.; Kato, M.; Fukumoto, H.; Kanie, M.; Sano, S.; Tokunaga, F.; Tanaka, K.; Iwai, K. A ubiquitin ligase complex assembles linear polyubiquitin chains. *EMBO J.* **2006**, *25* (20), 4877–4887.

(32) Tokunaga, F.; Sakata, S.; Saeki, Y.; Satomi, Y.; Kirisako, T.; Kamei, K.; Nakagawa, T.; Kato, M.; Murata, S.; Yamaoka, S.; Yamamoto, M.; Akira, S.; Takao, T.; Tanaka, K.; Iwai, K. Involvement of linear polyubiquitylation of NEMO in NF-κB activation. *Nat. Cell Biol.* **2009**, *11* (2), 123–132.

(33) Kruse, J. P.; Gu, W. Modes of p53 regulation. *Cell* **2009**, *137* (4), 609–622.

(34) Charvet, C.; Wissler, M.; Brauns-Schubert, P.; Wang, S. J.; Tang, Y.; Sigloch, F. C.; Mellert, H.; Brandenburg, M.; Lindner, S. E.; Breit, B.; Green, D. R.; McMahon, S. B.; Borner, C.; Gu, W.; Maurer, U. Phosphorylation of Tip60 by GSK-3 determines the induction of PUMA and apoptosis by p53. *Mol. Cell* **2011**, *42* (5), 584–96.

(35) Johnson, E. S. Protein modification by SUMO. *Annu. Rev. Biochem.* **2004**, *73*, 355–382.

(36) Choudhary, C.; Kumar, C.; Gnad, F.; Nielsen, M. L.; Rehman, M.; Walther, T. C.; Olsen, J. V.; Mann, M. Lysine acetylation targets protein complexes and co-regulates major cellular functions. *Science* **2009**, *325* (5942), 834–840.

(37) Gareau, J. R.; Lima, C. D. The SUMO pathway: emerging mechanisms that shape specificity, conjugation and recognition. *Nat. Rev. Mol. Cell. Biol.* **2010**, *11* (12), 861–871.

(38) Perry, A. S.; Watson, R. W.; Lawler, M.; Hollywood, D. The epigenome as a therapeutic target in prostate cancer. *Nat. Rev. Urol.* **2010**, *7* (12), 668–680.

(39) Wang, Q.; Zhang, Y.; Yang, C.; Xiong, H.; Lin, Y.; Yao, J.; Li, H.; Xie, L.; Zhao, W.; Yao, Y.; Ning, Z. B.; Zeng, R.; Xiong, Y.; Guan, K. L.; Zhao, S.; Zhao, G. P. Acetylation of metabolic enzymes coordinates carbon source utilization and metabolic flux. *Science* **2010**, *327* (5968), 1004–1007.

(40) Zhao, S.; Xu, W.; Jiang, W.; Yu, W.; Lin, Y.; Zhang, T.; Yao, J.; Zhou, L.; Zeng, Y.; Li, H.; Li, Y.; Shi, J.; An, W.; Hancock, S. M.; He, F.; Qin, L.; Chin, J.; Yang, P.; Chen, X.; Lei, Q.; Xiong, Y.; Guan, K. L. Regulation of cellular metabolism by protein lysine acetylation. *Science* **2010**, *327* (5968), 1000–1004.

(41) Margueron, R.; Reinberg, D. The Polycomb complex PRC2 and its mark in life. *Nature* **2011**, *469* (7330), 343–349.

(42) Watson, I. R.; Irwin, M. S.; Ohh, M. NEDD8 pathways in cancer, Sine Quibus Non. *Cancer Cell* **2011**, *19* (2), 168–176.

(43) Desterro, J. M.; Rodriguez, M. S.; Hay, R. T. SUMO-1 modification of IκBα inhibits NF-κB activation. *Mol. Cell* **1998**, *2* (2), 233–239.

(44) Kouzarides, T. Acetylation: a regulatory modification to rival phosphorylation? *EMBO J.* **2000**, *19* (6), 1176–1179.

(45) Papouli, E.; Chen, S.; Davies, A. A.; Huttner, D.; Krejci, L.; Sung, P.; Ulrich, H. D. Crosstalk between SUMO and ubiquitin on PCNA is mediated by recruitment of the helicase Srs2p. *Mol. Cell* **2005**, *19* (1), 123–133.

(46) Yang, X. J.; Seto, E. Lysine acetylation: codified crosstalk with other posttranslational modifications. *Mol. Cell* **2008**, *31* (4), 449–461.

(47) Wu, S. Y.; Chiang, C. M. Crosstalk between sumoylation and acetylation regulates p53-dependent chromatin transcription and DNA binding. *EMBO J.* **2009**, *28* (9), 1246–1259.

(48) Pagano, M.; Tam, S. W.; Theodoras, A. M.; Beer-Romero, P.; Del Sal, G.; Chau, V.; Yew, P. R.; Draetta, G. F.; Rolfe, M. Role of the ubiquitin-proteasome pathway in regulating abundance of the cyclin-dependent kinase inhibitor p27. *Science* **1995**, *269* (5224), 682–685.

(49) Nakayama, K. I.; Nakayama, K. Ubiquitin ligases: cell-cycle control and cancer. *Nat. Rev. Cancer* **2006**, *6* (5), 369–381.

(50) Shirane, M.; Harumiya, Y.; Ishida, N.; Hirai, A.; Miyamoto, C.; Hatakeyama, S.; Nakayama, K. I.; Kitagawa, M. Down-regulation of $p27^{Kip1}$ by two mechanisms, ubiquitin-mediated degradation and proteolytic processing. *J. Biol. Chem.* **1999**, *274* (20), 13886–13893.

Cell

# FBXL21 Regulates Oscillation of the Circadian Clock through Ubiquitination and Stabilization of Cryptochromes

Arisa Hirano,[1] Kanae Yumimoto,[2] Ryosuke Tsunematsu,[2] Masaki Matsumoto,[2] Masaaki Oyama,[3] Hiroko Kozuka-Hata,[3] Tomoki Nakagawa,[1] Darin Lanjakornsiripan,[1] Keiichi I. Nakayama,[2,*] and Yoshitaka Fukada[1,*]

[1]Department of Biophysics and Biochemistry, Graduate School of Science, The University of Tokyo, 7-3-1 Hongo, Bunkyo-ku, Tokyo 113-0033, Japan

[2]Department of Molecular and Cellular Biology, Medical Institute of Bioregulation, Kyushu University, 3-1-1 Maidashi, Higashi-ku, Fukuoka, Fukuoka 812-8582, Japan

[3]Medical Proteomics Laboratory, Institute of Medical Science,The University of Tokyo, 4-6-1 Shirokanedai, Minato-ku, Tokyo 108-8639, Japan

*Correspondence: nakayak1@bioreg.kyushu-u.ac.jp (K.I.N.), sfukada@mail.ecc.u-tokyo.ac.jp (Y.F.)

http://dx.doi.org/10.1016/j.cell.2013.01.054

## SUMMARY

In the mammalian circadian clockwork, CRY1 and CRY2 repressor proteins are regulated by posttranslational modifications for temporally coordinated transcription of clock genes. Previous studies revealed that FBXL3, an F-box-type E3 ligase, ubiquitinates CRYs and mediates their degradation. Here, we found that FBXL21 also ubiquitinates CRYs but counteracts FBXL3. *Fbxl21*$^{-/-}$ mice exhibited normal periodicity of wheel-running rhythms with compromised organization of daily activities, while an extremely long-period phenotype of *Fbxl3*$^{-/-}$ mice was attenuated in *Fbxl3/Fbxl21* double-knockout mice. The double knockout destabilized the behavioral rhythms progressively and sometimes elicited arrhythmicity. Surprisingly, FBXL21 stabilized CRYs and antagonized the destabilizing action by FBXL3. Predominantly cytosolic distribution of FBXL21 contrasts with nuclear localization of FBXL3. These results emphasize the physiological importance of antagonizing actions between FBXL21 and FBXL3 on CRYs, and their combined actions at different subcellular locations stabilize oscillation of the circadian clock.

## INTRODUCTION

Circadian rhythms with a period of approximately 24 hr are generated by an internal timekeeping mechanism referred to as the circadian clock (Takahashi, 1995, Dunlap, 1999). In mammals, the central circadian pacemaker in the hypothalamic suprachiasmatic nucleus (SCN) governs behavioral rhythms and coordinates peripheral clocks located in a variety of tissues (Schibler and Sassone-Corsi, 2002; Hastings et al., 2003). The mammalian circadian clocks are driven by a transcription-translation-based negative feedback loop. In the clockwork, CLOCK-BMAL1 heterodimers activate transcription of PERIODs (PER1-3) and CRYPTOCHROMEs (CRY1 and CRY2) through binding to E-box enhancer-elements (Gekakis et al., 1998; Bunger et al., 2000). Translated PER and CRY proteins associate with each other, translocate into the nucleus, and repress their own transcription through interaction with CLOCK-BMAL1 (Kume et al., 1999; Shearman et al., 2000). Among the clock proteins, CRY1 and CRY2 act as key players in the mammalian clockwork through their strong repressive activities on CLOCK-BMAL1-dependent transcription (Kume et al., 1999; van der Horst et al., 1999).

In addition to the transcriptional regulation, posttranslational modifications of clock proteins have critical roles for the circadian oscillation of the molecular clock (Toh et al., 2001; Gallego and Virshup, 2007; Nolan and Parsons, 2009; Reischl and Kramer, 2011). We previously reported a posttranslational mechanism regulating the stability of CRY2 protein. CRY2 is phosphorylated at Ser557 in a circadian manner in the mouse SCN and liver (Harada et al., 2005; Kurabayashi et al., 2006). The priming phosphorylation of CRY2 at Ser557 by DYRK1A allows subsequent phosphorylation at Ser553 by GSK-3β, and the two-step phosphorylation at the two neighboring Ser residues of CRY2 leads to its proteasomal degradation (Kurabayashi et al., 2010). On the other hand, CRY1 and CRY2 are ubiquitinated by the Skp1-Cul1-FBXL3 ($SCF^{FBXL3}$) ubiquitin ligase complex (Busino et al., 2007), and the interaction of CRYs with FBXL3, an F-box protein, is promoted by AMP-activated protein kinase (AMPK)-mediated phosphorylation of CRYs (Lamia et al., 2009). FBXL3-mediated ubiquitination of CRYs leads to their proteasomal degradation, and two point mutations in mouse *Fbxl3*, i.e., *After-hour* (*Afh*) and *Overtime* (*Ovtm*), each cause remarkable lengthening of the free-running period of the mouse behavioral rhythms (Siepka et al., 2007; Godinho et al., 2007). However, CRY2-FBXL3 interaction and FBXL3-mediated CRY2 degradation do not require Ser557/Ser553 phosphorylation of CRY2 (Kurabayashi et al., 2010). Thus, CRY proteins are subject

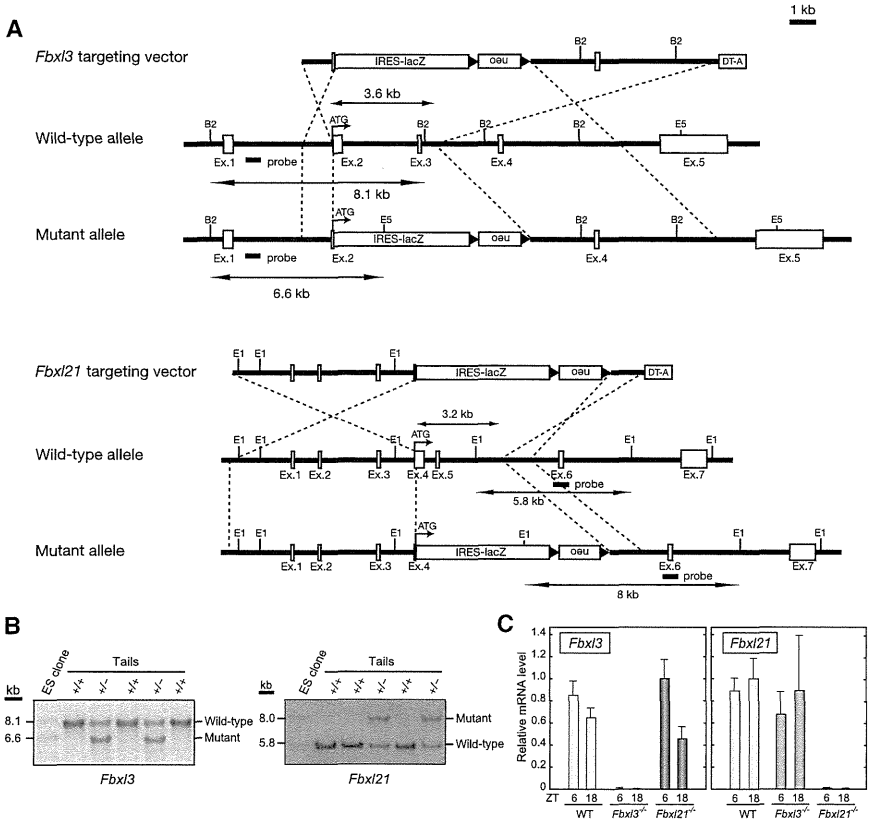


**Figure 1. Generation of *Fbxl3* and *Fbxl21* Knockout Mice**

(A) Targeting vectors for generation of *Fbxl3* knockout mice (*Fbxl3*$^{-/-}$) and *Fbxl21* knockout mice (*Fbxl21*$^{-/-}$).

(B) Southern blotting analysis of genomic DNA from tails of mice with the indicated genotypes for *Fbxl3* (left) or *Fbxl21* (right). The DNA was digested with BglII and EcoRV for *Fbxl3* or with EcoRI for *Fbxl21* genotyping. Hybridized probes are indicated in (A).

(C) *Fbxl3* (left) or *Fbxl21* (right) mRNA levels in the mouse liver quantified by real-time PCR. Data are means + SEM (n = 3) for wild-type and *Fbxl21*$^{-/-}$ mice and means + SD (n = 2) for *Fbxl3*$^{-/-}$ mice.

to degradation through at least two distinct pathways, postulating the involvement of another E3 ligase in the phosphorylation-dependent degradation of CRY2. Hence, we focused our attention on FBXL21, which is most similar in sequence to FBXL3 (84% amino acid sequence identity) among the F-box-type E3 ubiquitin ligase family (Jin et al., 2004; Dardente et al., 2008). Despite the similarity between these FBXL proteins, the physiological role of FBXL21 in the circadian clockwork remains to be elucidated (Dardente et al., 2008).

In this study, we show that FBXL21 ubiquitinates CRYs and that, surprisingly, FBXL21 stabilizes CRYs. FBXL21 localizes predominantly in the cytosol, whereas FBXL3 is present in the nucleus. Hence, the function and cellular distribution of FBXL21 form a sharp contrast with those of FBXL3 responsible for CRY protein degradation. The double knockout of *Fbxl3* and *Fbxl21* alleviated the circadian period-lengthening phenotype of *Fbxl3* knockout mice, further supporting their antagonizing actions on CRYs. Importantly, the double knockout destabilized the central clock in the SCN and progressively perturbed rhythmicity of the circadian behaviors in constant darkness. The antagonizing actions of *Fbxl3* and *Fbxl21* on CRY proteins have a critical role for robust oscillation of the mammalian circadian clock.

## RESULTS

### Generation of *Fbxl3* and *Fbxl21* Knockout Mice

*Afh* and *Ovtm* are two point-mutant alleles of *Fbxl3* (Siepka et al., 2007; Godinho et al., 2007). To evaluate the in vivo roles of *Fbxl3* and its closely related paralog, *Fbxl21*, we generated knockout mice lacking *Fbxl3* and/or *Fbxl21*. We created targeting vectors, in which IRES-*lacZ* and *neo* cassettes were introduced into the coding region of *Fbxl3* or *Fbxl21* gene (Figure 1A). Germline transmission of the mutant allele was confirmed by Southern blot analysis (Figure 1B). Heterozygous offspring crossed with C57BL/6 mice for at least seven generations were intercrossed to produce *Fbxl3* or *Fbxl21* knockout mice. In both cases, the genotypic distribution of the offspring followed Mendelian inheritance, and all the knockout mice used in the present study were normal in appearance. The messenger RNA (mRNA) levels of *Fbxl3* and *Fbxl21* in the liver of wild-type, *Fbxl3*$^{-/-}$, and *Fbxl21*$^{-/-}$ mice were analyzed by real-time PCR. *Fbxl3* or *Fbxl21* deficiency had no significant effect on the expression levels of *Fbxl21* or *Fbxl3*, respectively, when compared to their mRNA levels in the wild-type liver (Figure 1C).

### *Fbxl3* and *Fbxl21* Are Essential for Normal Behavioral Rhythms

We examined the effects of deficiencies of *Fbxl3* and/or *Fbxl21* on the behavioral rhythms of mice by monitoring their wheel-running activities (Figures 2A–2D). *Fbxl3* null mice apparently entrained to the 12L:12D (LD) cycle, although the onset of active phase was abnormally delayed from the light-to-dark transition (Figure 2E; Table S1 available online). In constant darkness (DD), *Fbxl3*-deficient mice showed rhythmic activities with a free-running period ($\tau_{DD}$) of 27.74 ± 0.20 hr (Figure 1F and Table S1), which was significantly longer than that of their wild-type littermates ($\tau_{DD}$: 23.77 ± 0.06 hr). Such an extremely long period in *Fbxl3*-deficient mice probably caused the delay of activity onset in LD. When transferred from DD to LD, 5 out of 14 *Fbxl3* knockout mice failed to entrain to the 24 hr cycle (Table S1) and apparently free ran as they did in DD (Figure 2C), a phenotype also observed in *Afh* mutant mice (Godinho et al., 2007). The circadian phenotype of *Fbxl3*-deficient mice ($\tau_{DD}$: 27.74 ± 0.20 hr) was more severe than those of *Fbxl3*$^{Afh/Afh}$ ($\tau_{DD}$: 26.5 hr, Godinho et al., 2007) and *Fbxl3*$^{Ovtm/Ovtm}$ ($\tau_{DD}$: 26.21 hr,

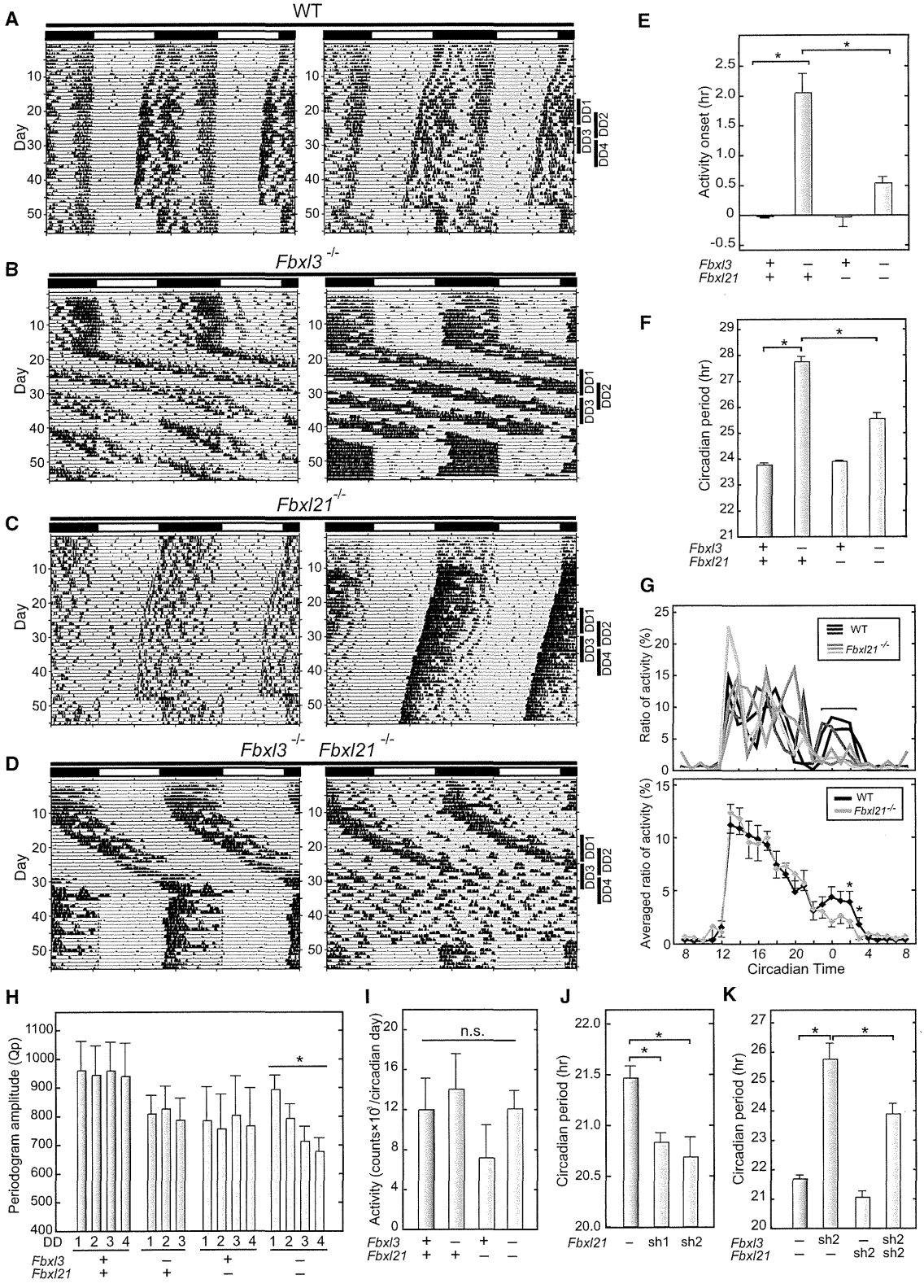


**Figure 2. Wheel-Running Activity of *Fbxl3* and *Fbxl21* Knockout Mice**

(A–D) Representative actograms of the wheel-running activities of wild-type (A), $Fbxl3^{-/-}$ $Fbxl21^{+/+}$ (B), $Fbxl3^{+/+}$ $Fbxl21^{-/-}$ (C), and $Fbxl3^{-/-}$ $Fbxl21^{-/-}$ (D). Mice were entrained to LD cycle for at least 5 weeks, transferred to DD, and then transferred to LD again.

*(legend continued on next page)*

Siepka et al., 2007). Thus, *Fbxl3* plays an important role in the regulation of the oscillation speed of the circadian clock in mice.

On the other hand, *Fbxl21*-deficient mice exhibited no significant difference from their wild-type littermates in both the free-running period in DD (Figure 2F) and activity onset in LD (Figure 2E). However, an alteration in the daily activities was obviously observed in *Fbxl21* null mice: During the active period, wild-type mice showed two peaks of activity bouts at early and late night, the latter of which was eliminated in *Fbxl21*-deficient mice (Figure 2G). This observation implies an involvement of *Fbxl21* in the SCN clock regulating temporal organization of the daily activities.

The strong phenotype of *Fbxl3* null mice in behavioral rhythm ($\tau_{DD}$: 27.74 ± 0.20 hr) was significantly attenuated in *Fbxl3/Fbxl21* double-knockout mice (Figures 2D and 2F; $\tau_{DD}$: 25.59 ± 0.15 hr). The abnormal delay of the activity onset observed in *Fbxl3* knockout mice in LD was also alleviated in the double-knockout mice (Figure 2E). However, we found that the double-knockout mice exhibited unstable behavioral rhythms in DD, although all of *Fbxl3* single-knockout mice showed rhythmic behaviors in DD: three out of ten *Fbxl3/Fbxl21* knockout mice were initially rhythmic but became arrhythmic within a few weeks after they were transferred to DD (Figure 2D, right panel; Table S1). We estimated the robustness of the behavioral rhythms for all the mice by the chi square periodogram procedure, where robustness is expressed as the Qp statistic reflecting the strength or regularity of a rhythm (Sokolove and Bushell, 1978). The double-knockout mice showed a progressive decline in Qp statistic during days 9–28 in DD (Figure 2H). This vulnerability was not observed in *Fbxl3* and *Fbxl21* single-knockout mice (Figure 2H; Table S1). It is therefore evident that *Fbxl3/Fbxl21* double deficiency destabilized the circadian oscillator in the SCN with no significant effect on the daily levels of wheel-running activity (Figure 2I). We conclude that the combined actions of *Fbxl21* and *Fbxl3* play a key role in the maintenance of both the speed and the robustness of the circadian clock oscillation.

### *Fbxl21* Regulates the Oscillation Speed of Cellular Clocks

A role of *Fbxl21* in the cellular clock was investigated in NIH 3T3 cells. To monitor the cellular rhythms, we introduced a luciferase reporter under the regulation of *Bmal1* promoter into the cultured cells by transient transfection. Silencing of *Fbxl21* was performed by cotransfection of an expression plasmid of small hairpin RNA (shRNA) sh21-1 or sh21-2 while *Fbxl3* was knocked down with sh3-1 or sh3-2 as described by Busino et al. (2007). Among them, sh3-2 and sh21-2 abrogated the expression of FBXL3 and FBXL21, respectively, and showed no significant crossover effects with each other (Figure S1A). We found that silencing of the *Fbxl21* gene significantly shortened the period of the cellular rhythm (Figures 2J and S1B). This period-shortening phenotype was not observed in the behavioral rhythms of *Fbxl21*-deficient mice (Figure 2F). Generally, the behavioral rhythms are only marginally affected by molecular defects in clock components due to the strong coupling among the SCN neurons, whereas the phenotypes often become manifest in the circadian rhythms of dispersed cells in culture (Liu et al., 2007). It is likely that the effect of *Fbxl21* deficiency, i.e., speeding up of the molecular oscillation, is masked by the tight neuronal coupling in the SCN. On the other hand, *Fbxl3* knockdown remarkably lengthened the periods, which were conversely shortened by additional knockdown of *Fbxl21* (Figures 2K and S1B). These results are consistent with the behavioral phenotypes of the knockout mice.

### Altered Molecular Rhythms in *Fbxl21* Knockout Mice

To investigate how *Fbxl21* deficiency affects the circadian clockwork, we synchronized the cellular clocks in mouse embryonic fibroblasts (MEFs) by a pulse treatment with dexamethasone (Dex). We found that CRY1 and CRY2 protein levels in *Fbxl21*-deficient MEFs were decreased and showed circadian oscillation with reduced amplitudes as compared with those in wild-type MEFs (Figures 3A and 3B). On the other hand, the peak mRNA levels of *Cry1*, *Cry2*, and *Per1* were increased in *Fbxl21* null MEFs (Figure 3C). These results suggest destabilization of CRY proteins in *Fbxl21*-deficient MEFs. In contrast, the mRNA levels of *Dbp* were decreased and *Bmal1* mRNA levels were elevated throughout the day (Figure 3C). Although *Fbxl21*-deficient mice showed rhythmic behaviors with a period indistinguishable from that of wild-type mice (Figure 2C), transcriptional control of the clock genes is remarkably perturbed in the absence of *Fbxl21*. These molecular phenotypes can be at least in part attributable to the dysregulation of CRY1 and CRY2 in *Fbxl21*-deficient cells.

(E) Activity onset in LD cycle. The time of activity onset during the 5 days in LD just before the transition to DD was determined by ClockLab software. The means of the onset times relative to the LD transition time were plotted. Error bars show SEM. *$p < 0.05$ by Tukey's test.

(F) Circadian periods of free-running activities in DD determined by chi-square periodogram. Data from days 8 through 21 in DD were used for the calculation of the circadian periods. Error bars show SEM. *$p < 0.05$ by Tukey's test.

(G) Activity profiles of *Fbxl21*$^{-/-}$ mice across the day. (Upper panel) Typical activity profiles of wild-type and *Fbxl21*$^{-/-}$ mice in DD. (Lower panel) The ratios of the hourly activities relative to the daily total activity in DD of every mouse for each genotype were shown with error bars of SEM. *$p < 0.05$ by Tukey's test. The activity onset time was defined as circadian time 12.

(H) Temporal changes in periodogram amplitude (Qp) of the wheel-running activity rhythms of the knockout mice in DD. The Qp values were determined from the activity data during the four overlapping periods of 8 days in DD (DD1: days 9–16, DD2: days 13–20, DD3: days 17–24 and DD4: days 21–28) by chi-square periodogram by using ClockLab software (Actimetrics). Error bars show SEM. *$p < 0.05$ by one-way ANOVA.

(I) The total numbers of the wheel revolutions per circadian cycle were counted during 2 weeks (days 8–21) in DD. Error bars show SEM, and n.s. indicates not significant ($p > 0.05$ by one-way ANOVA).

(J and K) Circadian periods of cellular rhythms in culture. NIH 3T3 cells were cotransfected with a luciferase reporter (*Bmal1*us0.3-luc; Kon et al., 2008) and shRNA vectors targeting *Fbxl*s (J, *Fbxl21*; K, *Fbxl3* and/or *Fbxl21*). Forty-eight hours after the transfection, the cells were treated with 0.1 μM dexamethasone for 2 hr to synchronize the cellular rhythms. The culture medium was then changed to the recording medium for recording bioluminescence signals. Circadian periods were calculated by using the data from the 2nd to the 4th peak. Error bars show SEM (n = 4, *$p < 0.05$ by Tukey's test). See also Figure S1 and Table S1.

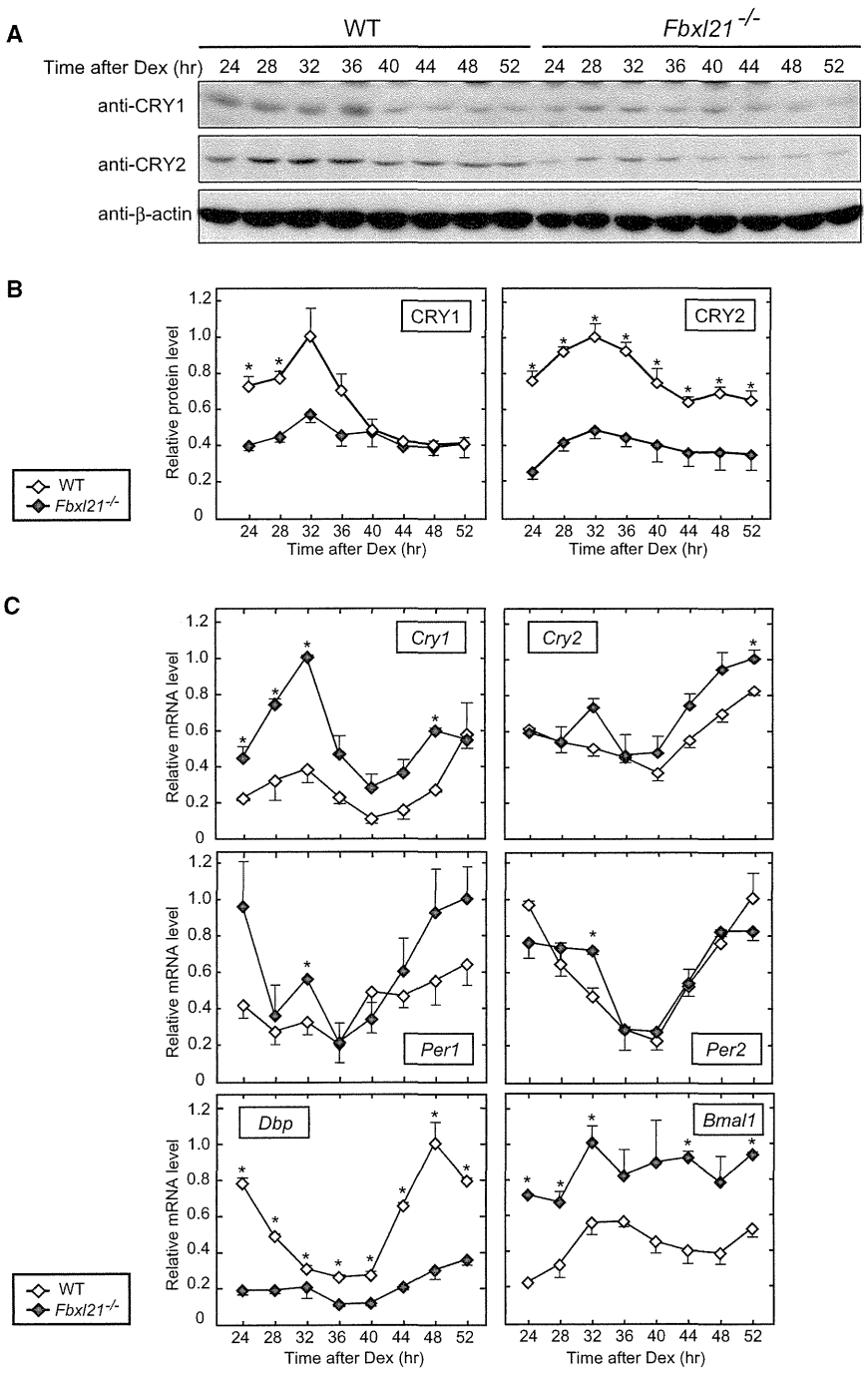


**Figure 3. Circadian Expression of CRY Proteins and Clock Genes in *Fbxl21* Knockout Mice**

(A) Temporal changes in CRY1 and CRY2 protein levels in *Fbxl21*$^{-/-}$ MEFs. Cellular rhythms of MEFs were synchronized by 2 hr pulse treatment of 0.1 μM dexamethasone. The cells were harvested at 4 hr intervals followed by immunoblotting with CRY1 or CRY2 antibody.

(B) The band densities of CRY1 or CRY2 in (A) within a single blot were shown as values relative to their average intensity in the blot, and the highest value was set at 1.0. Data taken from three independent experiments (i.e. three blots) were averaged and shown with error bars of SEM (n = 3, *p < 0.05 by Student's t test).

(C) Temporal changes in mRNA levels of clock genes in *Fbxl21*$^{-/-}$ MEFs. Cellular rhythms of MEFs were synchronized and total RNA was prepared at 4 hr intervals. The mRNA levels of *Cry1*, *Cry2*, *Per1*, *Per2*, *Dbp*, and *Bmal1* were quantified by real-time PCR, and the highest value among the samples was set at 1.0. Data are means with SEM (n = 3, *p < 0.05 by Student's t test).

## FBXL21 Interacts with CRY Proteins

The abnormalities in temporal changes of CRY1 and CRY2 protein levels in *Fbxl21*-deficient MEFs suggest that FBXL21 shares with FBXL3 a regulatory mechanism determining CRY protein levels. We first examined the interaction of FBXL21 with CRY1 and CRY2 in cultured cells. HEK293T17 cells were transfected with expression constructs of myc-CRYs and Flag-FBXLs. We found that, just like Flag-FBXL3, Flag-FBXL21 was coimmunoprecipitated with myc-CRY1 and myc-CRY2 (Figure 4A). The interaction between myc-CRY1 and Flag-FBXL21 was verified by coimmunoprecipitation of myc-CRY1 with Flag-FBXL21 (Figure 4B).

## FBXL21 Forms an SCF Complex

Members of the F-box-type E3 ubiquitin ligase family have a conserved F-box domain and a substrate recognition domain that is divergent among the members. The F-box domain is important for the formation of a Skp1-Cul1-F-box protein (SCF) complex to exert E3 ligase activity (Cardozo and Pagano, 2004). To investigate E3 ligase activity of FBXL21, we asked whether FBXL21 forms an SCF complex. Recently, the authors K.Y. and K.I.N. found that FBXL3 forms an SCF complex in a manner dependent on CRY protein (unpublished data). Based on this observation, we coexpressed myc-CRY1 or myc-CRY2 with Flag-FBXL21 or Flag-FBXL3 in HEK293T17 cells. Each myc-CRY facilitated the interaction of Skp1 and Cul1 not only with Flag-FBXL3 but also with Flag-FBXL21 (Figure 4C). It is most likely that FBXL3 and FBXL21 share the same domain for CRY binding and that the E3 ligase activities of these F-box proteins are regulated in a circadian manner through the dynamic change in CRY protein levels. Here, we noticed that Cul1 band in the precipitate with FBXLs was upshifted from the Cul1 band in the input (Figure 4C). Because NEDD8 modification of Cul1 is known to activate the SCF complex by recruiting an E2 enzyme (Pan et al., 2004), the upshifted Cul1 band might

represent its neddylated state in the SCF complex containing CRYs.

**FBXL21 Ubiquitinates CRY Proteins**

By using in vitro ubiquitination assay, we examined FBXL21-catalyzed ubiquitination of CRY1 in the presence of 1 of 17 E2 enzymes. We found that UBE2A or UBE2D (D1-D3: UbcH5a-5c) cooperated with not only FBXL3 but also FBXL21 in ubiquitinating CRY1 (Figures 4D and S2A). We also found an in vivo ubiquitination assay that cotransfection of Flag-FBXL3 or Flag-FBXL21 enhanced myc-CRY1 ubiquitination in HEK293T17 cells (Figures 4E and S2B) and NIH 3T3 cells (Figure S2C). Among various linkage types of ubiquitin chains, K48-linked polyubiquitination is primarily known as the protein degradation signal (Behrends and Harper, 2011). The linkage modes of FBXL21- and FBXL3-mediated ubiquitination were examined by using a mutant ubiquitin, HA-K48-Ub, in which all Lys residues except for K48 were mutated to Arg. Coexpression of Flag-FBXL3 or Flag-FBXL21 with HA-wt-Ub promoted myc-CRY1 ubiquitination to be nearly comparable to each other. On the other hand, coexpression with HA-K48-Ub attenuated myc-CRY1 ubiquitination catalyzed by FBXL21 when compared to that achieved with FBXL3 (Figure 4F). These results suggest that FBXL3 and FBXL21 elongate different types of ubiquitin chains, at least in terms of their dependence on K48 linkage. Further studies using a series of other mutant ubiquitins (such as K11-Ub, K48R-Ub, and K63-Ub) would help to identify the linkage mode of ubiquitin chains formed by FBXL21. We then asked whether CRYs are endogenous substrates of FBXL21 in NIH 3T3 cells by knockdown of *Fbxl21*. Silencing of *Fbxl21* or *Fbxl3* reduced the ubiquitinated levels of myc-CRY1 in NIH 3T3 cells (Figures 4G and S2D). These results indicate that CRY1 is an endogenous substrate for FBXL21- and FBXL3-catalyzed ubiquitination.

**FBXL21 Stabilizes CRY Proteins**

Ubiquitination of proteins confers various regulations on modified proteins, such as protein stability, signal transduction, enzymatic activity, and subcellular localization (Chen and Sun, 2009), whereas F-box protein-mediated ubiquitination predominantly leads the substrates to proteasomal degradation (Cardozo and Pagano, 2004). We asked whether FBXL21 regulates stabilities of CRYs by quantifying the steady-state protein levels of Flag-His-myc-tagged CRY1 (FHM-CRY1) when FBXL21 and/or FBXL3 are either overexpressed or knocked down. Overexpression of Flag-FBXL3 in HEK293T17 cells decreased FHM-CRY1 protein levels, indicating that FBXL3 promotes CRY1 degradation (Figure 5A). In contrast, overexpression of Flag-FBXL21 remarkably elevated FHM-CRY1 levels (Figure 5A). Coexpression of Flag-FBXL3 and Flag-FBXL21 restored FHM-CRY1 levels (Figure 5A), and the restoration was dose dependent for Flag-FBXL21 (Figure 5B). Similar results were obtained in experiments performed with FHM-CRY1 in NIH 3T3 cells (Figure S3A) or with FHM-CRY2 in NIH 3T3 cells (Figure S3B), suggesting that FBXL3 and FBXL21 act on CRY proteins in a mutually antagonizing manner. Myc-PER2 also binds to Flag-FBXL3 and Flag-FBXL21, possibly via indirect interaction through CRYs (Figure S3C), but myc-PER2 protein levels were mostly unaffected by coexpression with Flag-FBXL21 and/or Flag-FBXL3 (Figure S3D). An increase in Flag-FBXL21 levels had no discernible effect on Flag-FBXL3 level (Figures 5A and 5B), eliminating the possibility that the effect of overexpressed Flag-FBXL21 on FHM-CRY1 was due to the change of FBXL3 levels. Meanwhile, knockdown of *Fbxl21* by sh21-2 in NIH 3T3 cells resulted in a decrease in the steady-state levels of FHM-CRY1, whereas knockdown of *Fbxl3* increased FHM-CRY1 levels (Figure 5C). Collectively, these results indicate that CRY1 levels are regulated by FBXL21 and FBXL3 antagonistically, where FBXL21 increases CRY1 levels probably through its stabilization.

To confirm that the stability of CRY proteins is increased by FBXL21, we investigated the degradation rate of myc-CRY1 protein in cultured cells. HEK293T17 cells expressing myc-CRY1 and Flag-FBXLs were treated with cycloheximide (CHX) for 3–6 hr. Expression of Flag-FBXL3 increased myc-CRY1 degradation rate, while Flag-FBXL21 expression significantly suppressed the degradation (Figure 5D). Coexpression of Flag-FBXL3 and FBXL21 attenuated FBXL3-dependent myc-CRY1 degradation. A similar set of experiments in NIH 3T3 cells confirmed the stabilizing effect of Flag-FBXL21 on FHM-CRY1 (Figures S3E and S3F). The half-life of luciferase activity of CRY1-LUC fusion protein was markedly increased (~two-fold) by Flag-FBXL21 expression (Figure 5E), whereas the lifetime of LUC itself was unaffected by Flag-FBXL3 or Flag-FBXL21 (Figure S3G). In *Fbxl21* knockout MEFs, by contrast, the decay of CRY2 was significantly faster than that in wild-type MEFs (Figure 5F). These results demonstrate an important role of FBXL21 in CRY protein stabilization, which antagonizes the destabilizing action by FBXL3.

**Ubiquitination Sites in CRY1 and CRY2**

We investigated ubiquitination sites in CRY proteins by shotgun proteomic analysis of FHM-tagged CRY1 or CRY2, each of which was immunopurified from the lysates of NIH 3T3 cells (Table 1). We found a series of ubiquitinated residues in FHM-CRYs: K159, K329, and K485 in FHM-CRY1 and K125, K241, K347, K474, and K503 in FHM-CRY2 (Figure 6A, K is labeled with an asterisk). In addition, we found ubiquitinated residues in ubiquitin copurifed with FHM-CRYs: K11, K48, and K63 (Table 1). A recent study of human ubiquitin-modified proteome identified ubiquitinated residues K329 and K442 in CRY1 and K241 and K474 in CRY2 (Kim et al., 2011). The present analysis covered three out of the four ubiquitinated sites reported for human CRYs and revealed two and three additional sites in mouse CRY1 and CRY2, respectively. CRY proteins are multiply ubiquitinated in vivo, suggesting the possibility that FBXL21 and FBXL3 each catalyzes ubiquitination at a distinct subset of Lys residues in CRYs. To examine whether ubiquitination of these sites is essential for FBXL21-mediated stabilization of CRY1, we generated four mutants of myc-CRY1 (mut1–4) by introducing a K-to-R mutation, respectively, at K107, K329, K456, and K485, Lys residues which are ubiquitinated in CRY1 and/or CRY2 and are conserved between CRY1 and CRY2 (Figure 6A). Among these mutants, mut1-CRY1 (K107R) protein levels were sensitive to FBXL3-dependent degradation and, by contrast, they were unaffected by coexpression of FBXL21 in